Light-evoked activity and BDNF regulate mitochondrial dynamics and mitochondrial localized translation.

Alex Kreymerman[1,2*], Jessica E. Weinstein[2*], Sahil H. Shah[1,3], David N. Buickians[1], Anne Faust[4], Yolandi Van Der Merwe[4], Michael M. Nahmou[1], In-Jae Cho[1], Star K. Huynh[1], Sonya Verma[1], Xiao-Lu Xin[2], Michael B. Steketee[2,4], Jeffrey L. Goldberg[1]

1. Byers Eye Institute, Stanford University, Palo Alto, CA 94303
2. University of Miami Miller School of Medicine, Miami, FL 33136
3. Medical Scientist Training Program, University of California, San Diego, CA 92093
4. Department of Ophthalmology and McGowan Institute for Regenerative Medicine, University of Pittsburgh, Pittsburgh, PA 15213

*These authors contributed equally.

Address correspondence to:
Jeffrey L. Goldberg
Byers Eye Institute
Stanford University
2452 Watson Ct
Palo Alto, CA 94303

Abstract

Mitochondria coordinate diverse functions within neurites, including signaling events for axonal maintenance, and degeneration. However, less is known about the role of mitochondria in axon development and maturation. Here we find that in maturing retinal ganglion cells (RGCs) in vivo, axonal mitochondria increase in size, number, and total area throughout development. We demonstrate through multiple approaches in vivo that the mechanism underlying these mitochondrial changes are dependent on eye opening and associated neuronal activity, which can be mimicked by brain derived neurotrophic factor (BDNF). We report downstream gene and protein expression changes consistent with mitochondrial biogenesis and energetics pathways, and present evidence that the associated transcripts are localized and translated at mitochondria within axons in an activity-dependent manner. Together these data support a novel model for mitochondrial-localized translation in support of intra-axonal mitochondrial dynamics and axonal maturation.

Introduction

Neurons are among the highest metabolically active cell types in the body. This is due in part to mitochondrial oxidative phosphorylation highly coupled with the energy demand generated by electrophysiologic activity and associated signaling[1-3]. Beyond ATP production, mitochondrial activities such as calcium homeostasis, fatty acid oxidation, secondary messenger and signaling pathway modulation also participate in supporting neurons and their extensive axonal compartments[4]. Mitochondrial activities are critically dependent on the expression and assembly of approximately 600-1500 proteins encoded in the nucleus[5-12], yet mitochondria can be separated down the axon by a meter or more from the cell body[13].

As a result, such cells have evolved unique mechanisms for maintaining continuous communication between mitochondria and the nucleus[14]. These include shuttling mitochondria and their nuclear-encoded proteins up and down axons using motor proteins kinesins and dyneins[15-18]. Transported mitochondria are also capable of undergoing fusion or fission with neighboring mitochondria, acquiring or shedding genetic material and proteins[19]. Finally, new mitochondria can also be assembled and packaged with nuclear and mitochondrial encoded proteins, in a process known as mitochondrial biogenesis. This process takes place in the perinuclear space and within axons, leading to increased numbers of mitochondria in neuronal compartments[20-22]. Together these changes in mitochondrial localization, size and total cellular volume are referred to as mitochondrial dynamics.

An additional mechanism implicated in supplying nuclear proteins to distal axonal mitochondria is the transport and then local translation of RNA in axonal compartments (reviewed elsewhere[23]). Interestingly, many investigations indicate that a consistent and major portion of axon-localized transcripts encode nuclear proteins that regulate mitochondrial functions[24-27]. Additionally, nuclear-encoded mitochondrial transcripts have been shown to physically localize on/in mitochondrial membranes[28-32], with further evidence suggesting that mitochondria can act as local translation sites[33-35]. However, it is not yet known how such localization is regulated. Here we find that developmental changes in axonal mitochondria are regulated by activity in vivo, and explore associated regulation of mRNA expression and localization by activity in RGCs in vitro.

Results

68 Mitochondrial networks reorganize at the time of eye opening

69 We first studied mitochondrial organization in RGC axons in transgenic mice expressing cyan
70 fluorescent protein (CFP) fused to the COX8a mitochondrial targeting sequence under control of
71 the Thy-1 promoter (Thy1-CFP/COX8A). In this mouse, approximately 5% of RGCs express the
72 CFP/COX8a transgene, permitting visualization and quantification of mitochondria in RGC axons
73 (Figure 1A,B). We used this mouse model to investigate axon-specific mitochondrial networks at
74 postnatal (P) days 9, 12, 15, and 45, as RGCs experience significant developmental changes
75 through this time period[28-31,36-39,40-44]. Of note, these time points also follow the period of
76 developmental cell death in RGCs, which peaks at P5 in mice [45-47], thus allowing for the
77 identification of mitochondrial changes independent of cell death signaling, which can influence
78 mitochondrial morphology[48,49]. Analysis of CFP-labeled mitochondria in whole mount retinas and
79 optic nerves by confocal microscopy revealed significant reorganization in RGC axons throughout
80 postnatal development (Figure 1B). Overall, mitochondria increased in size, number, and occupied
81 a greater percentage of axonal area from P9 to P45 (Figure 1C-E). Interestingly, within a relatively
82 short window of development, around eye opening (P12/13 to P15), mitochondrial size, number,
83 and occupied area increased in both RGC retinal and optic nerve axon segments, with optic nerve
84 mitochondria experiencing the greatest change during this time window.
85
86 Although Thy-1 gene expression peaks around P12 in RGCs and continues to be stably expressed
87 throughout adulthood[50], and thus Thy-1 promoter-related artifacts are unlikely, mitochondria size
88 changes from P12-P15 were also confirmed by transmission electron microscopy (TEM; Figure
89 2). Specifically, mitochondrial size, number, and occupied area increased in RGC axons from P12
90 to P15 by 25%, 105%, and 31% respectively (Figure 2B, C, D). Thus by both fluorescence and

TEM imaging, RGC axon mitochondrial size, number, and occupied area increase during this developmental window.

Eye opening regulates mitochondrial networks

As eye opening occurs between P12-P15 with a concomitant significant increase in visual activity, we asked whether the mitochondrial morphological changes are dependent on eye opening in CFP-COX8a mice with surgically premature or delayed eye opening. (Figure 3A). For premature eye opening, we surgically opened the P10 eyelid margin, two days prior to normal eye opening, and allowed animals to mature to P12. We found increases in mitochondrial size, number and occupied area in retinal and optic nerve axons compared to unopened P12 eyes (Figure 3B, C, D). Thus eye opening accelerates the mitochondrial morphology changes identified in normal development.

Conversely, to determine if eye opening is necessary for the developmental increases in mitochondrial size, number, and occupied area from P12-15, we delayed eye opening by suturing eyelids shut at P11, prior to natural eye opening, then allowed mice to mature to P15, delaying eye opening by 2-3 days (Figure 3A). Compared to age-matched controls, the delayed eye opening model led to significant decreases in all mitochondrial measurements (Figure 3B, C, D), in most cases back to levels found in P12 animals. Thus, these data suggest that the process of eye opening is sufficient and necessary for the mitochondrial network increases found from P12-15.

RGC activity and BDNF regulate mitochondrial networks

These findings suggested the hypothesis that light-stimulated electrical activity in axons (i.e., action potentials) contribute to the observed changes in axon mitochondrial distribution and

morphology. To test the contribution of electrical activity to axonal mitochondrial changes during the period of eye opening, we pharmacologically inhibited both spontaneous and light-evoked electrical activity in RGCs by intravitreally injecting tetrodotoxin (TTX)[51] prior to eye opening at P11 and again after eye opening at P13, followed by mitochondrial quantification at P15. We found that TTX but not control vehicle injection inhibited mitochondrial increases in size in retinal and optic nerve axons (Figure 4A, B), and mitochondrial number and occupied area only in the optic nerve portion of RGC axons (Figure 4C, D), in all cases to levels equivalent to vehicle injected P12 animals. Thus RGC electrical activity is a significant contributor to mitochondrial network changes that occur concomitant with eye opening. However, discrepancies in mitochondrial numbers and area within retinal versus optic nerve axons likely indicate additional regulation that contributes to mitochondrial dynamics during this period.

Downstream of electrical activity, BDNF expression has been shown to be regulated by eye opening and to be blocked by TTX injection[36], and to modulate mitochondrial dynamics[36,52-55]. To determine whether BDNF could rescue the inhibitory effects of TTX on mitochondrial networks, BDNF and TTX were co-injected at P11 and again at P13, and mitochondrial parameters were measured at P15. BDNF was capable of significantly reversing the TTX-induced decreases in mitochondrial size, and showed a non-significant trend towards such rescue in mitochondrial number and occupied area in optic nerve axons (Figure 4B-D). Of note, this rescue effect of BDNF was only detected in the optic nerve but not retinal axons (Figure 4A), suggesting again that different mechanisms regulate mitochondrial dynamics in a compartment-specific manner within the axon. Furthermore, when BDNF was injected at P10 and mitochondrial parameters were measured at P12, BDNF did not increase mitochondrial size, number or area on its own (Figure

137 4A-D). Nonetheless, these data suggest that activity and BDNF are both critical in regulating the
138 morphology and distribution of optic nerve axon mitochondria during this stage of visual system
139 development.
140
141 Activity and BDNF regulate the expression of nuclear encoded mitochondrial genes
142 To investigate molecular mechanisms associated with activity and BDNF, we explored the
143 transcriptional influence of exogenously added BDNF and TTX on nuclear-encoded mitochondrial
144 gene expression in RGCs. To accomplish this, we injected TTX and/or BDNF in combination or
145 alone at P11 and P13, acutely purified RGCs from P15 retinas, and extracted RNA for qRT-PCR
146 gene arrays. We then analyzed expression data and conducted pathway analysis. Major upstream
147 regulators were identified by probing the gene expression sets for targets of known regulators, and
148 then filtering for genes whose expression was concordant with the inhibitory effects of TTX and
149 subsequent rescue with BDNF on mitochondrial morphology and distribution (Figure 5A). The
150 resulting analysis revealed that PGC1-α and RICTOR, master mitochondrial dynamics and
151 energetics modulators, were putative upstream regulators of genes modulated by TTX and/or
152 BDNF (Figure 5B, C). For many mitochondria genes regulated by RICTOR and PGC1-α, TTX
153 and BDNF showed opposing effects on expression. In most cases, the gene expression profile of
154 TTX+BDNF mimicked that of BDNF alone, suggesting BDNF's effects on gene expression were
155 dominant over effects of TTX and placing BDNF downstream of activity. Furthermore, BDNF
156 increased basal and maximum respiratory capacity in purified RGCs in vitro even in the presence
157 of TTX (Figure 5D), consistent with pathways predicted by these gene expression changes.
158 Ontological analysis of these gene expression datasets suggested opposing functions between
159 BDNF and TTX, with fission/fusion and mitochondrial biogenesis pathways induced by BDNF

and suppressed by TTX (Figure 5E, F), consistent with our *in vivo* data.

Activity regulates mitochondrial associated local translation and mitochondrial dynamics

Our gene arrays showed that expression of many of the mitochondrial genes assayed were suppressed by TTX-mediated inhibition of activity. To investigate whether transcription or translation activity were being globally downregulated in RGCs by activity inhibition, we treated RGCs with 5-ethynyluridine (EU), a uridine analog, or O-propargyl-puromycin (OPP), a puromycin analog. These molecules readily incorporate into newly synthesized RNAs (with EU) or proteins (with OPP), and can be conjugated to fluorophores with click chemistry to visualize the location and relative amount of synthesis taking place within cells[56,57]. Using this approach, we first tested whether TTX inhibited transcription or translation by intravitreally injecting TTX at P11 and P13, and then pulsing with EU or OPP at P15 for 1hr. Upon visualization, no detectable differences in signal intensity from EU or OPP were identified in retinas (Figure 6A), suggesting that transcription and translation where not broadly inhibited by activity suppression.

However, because of the potential variability with labeling efficiency, either from injection site differences, variations in injection volumes, and/or kinetics of intravitreal injection dispersion, we followed up in vivo experiments with in vitro approaches where EU and OPP labeling can be better controlled and quantified. For in vitro approaches, RGCs were isolated to 99% purity by immunopanning from early postnatal mouse retinas and seeded at low density, allowing for the visualization of individual cells and neurites. Then, cells were virally transduced to fluorescently label mitochondria with a Cox8a targeted dsRED, cultured for 48hrs, treated with TTX for 2hrs, and finally pulsed for 15 min or 1hr with OPP or EU, respectively. The cells were treated with

183 TTX for a shorter period of time than during in-vivo experiments to avoid significant changes in
184 viability, which at early postnatal days has the potential to decrease cell survival, unlike the in vivo
185 time points tested[58]. However, no detectable decrease in viability after 2hr of TTX incubation was
186 detected (Figure 6B). In RGCs in vitro, we again found cells with intensely labeled peri-nuclear
187 regions, but no discernable differences in new transcript or protein levels in the cell body regions
188 (Figure 6C), similar to in vivo experiments. Interestingly, in OPP-treated cells, obvious puncta
189 were also visible in axonal segments. These puncta appeared scattered throughout distal axon
190 segments in axonal tips, with varying sizes and numbers (Figure 6D). To see if activity inhibition
191 by TTX could influence the presence of these axon-localized OPP puncta, we quantified the
192 abundance of OPP sites within axonal segments, and found that TTX-treated axons demonstrate
193 significant decreases (~70%) in the number of OPP puncta as compared to controls, similar to the
194 effects of translational inhibitor cycloheximide (Figure 6E), suggesting that activity regulates
195 axon-localized protein synthesis. Note that these changes in puncta number are not likely due to
196 decreased transport of newly synthesized proteins from the cell body, as the rate of soluble protein
197 transport is less than 0.1 µm/s (or 90 µm in 15 min) and would be an unlikely captured change
198 within the assay window in distal RGC axons[59], which are typically longer than 600µm at 48hrs
199 of culture in these cells[60].
200
201 Axon-localized protein translation has been previously described[31], but to further examine axon
202 localized OPP puncta we immunostained cells with an antibody against cytoplasmic ribosomal
203 protein S3, an integral component of the 40s-ribosomal subunit translation initiation site[61]. In these
204 cells, we found a significant level of co-localization of ribosomal protein S3 with OPP puncta and
205 interestingly a large majority of these OPP puncta also colocalized with mitochondria (Figure

206 6F,G), suggesting that the detected axon-localized OPP puncta active local translation sites are
207 often at or near mitochondria. Similar to our in vivo results, we further found that mitochondrial
208 size decreased in TTX-treated RGCs (Figure 6H) and was increased in the presence of BDNF,
209 which was dominant over the effect of TTX, with increases or decreases in mitochondrial size
210 correlating with increases or decreases in OPP-to-mitochondria localization (.499 r) (Figure 6J).
211 Of note, these puncta were not visible in EU-treated cells, which is either a reflection of the
212 abundance of RNA within axons or an indication of detection limitations. Thus new protein
213 synthesis is detected at mitochondria and together with mitochondrial network size shows a
214 dependence on electrical activity in RGC axons.
215
216 RNA binding proteins tether nuclear encoded mitochondrial mRNA to mitochondria
217 To investigate the potential for mitochondria to act as docking sites for nuclear-encoded
218 mitochondrial mRNA and new protein translation and, we conducted proteomic and qRT-PCR
219 experiments on mitochondria purified from optic nerves or retinas. Briefly, isolation of axonal
220 mitochondria was performed by incubating homogenized whole optic nerve tissue with a
221 magnetically conjugated Translocase Of Outer Mitochondrial Membrane 22 (TOM22) antibody.
222 Then, homogenates were passed through magnetic columns to remove cytosolic contaminants,
223 followed by extensive washing, elution, and the pelleting of mitochondria[62] (Figure 7A). We used
224 a number of approaches to validate this relatively novel purification protocol. First, isolated
225 mitochondria were examined by SEM and TEM, which showed that mitochondrial membranes
226 and cristae architecture were structurally maintained after isolation with dark puncta visible on the
227 outside of mitochondria (Figure 7B), representing nanoparticle-bound TOM22 and confirming the
228 integrity of outer mitochondrial membranes after isolation. On western blots, isolated

mitochondria maintained proteins from all complexes in the electron transport chain (Figure 7C) and inner and outer membrane integrity proteins (Figure 7D) but no detectable cytoplasmic GAPDH (Figure 7E). Of note, supernatant fractions from TOM22-purified mitochondria, which would reflect TOM22-bound membranes from ruptured, non-intact mitochondria, had no detectable ETC or membrane integrity proteins (Figure 7C, D), suggesting that nearly all TOM22-purified mitochondria were intact and captured in the pellet fraction. Finally, TOM22-selected optic nerve mitochondria were isolated from Thy-1-CFP/COX8a mice and further purified to axon-specific mitochondria through a traditional fluorescence acquired cell sorting (FACS) machine. In all FACs assays, mitochondria from Thy-1-CFP/COX8a mice retained membrane integrity proteins, detected by western blot (Figure 7F), and CFP positivity, detected by mitotracker-CMXROS co-staining(Figure 7G). Furthermore, isolated CFP^{+} mitochondria maintained high membrane potentials and readily took up JC-1, forming distinct populations of red shifted J-aggregate-retaining mitochondria (Figure 7H) that lost polarization in response to a membrane potential uncoupler, carbonyl cyanide-*4*-(trifluoromethoxy) phenylhydrazone (FCCP) (Figure 7I, J). Overall, these data suggest that isolating optic nerve axon mitochondria via magnetic columns and FACS yields relatively pure and structurally intact mitochondria, with surface and internal proteins and functional polarization maintained throughout the procedure.

We next examined these purified mitochondria for association with nuclear-encoded RNA binding proteins and translation-associated proteins from 3 young mouse optic nerves and also whole retinas by mass spectrometry, which yielded a total of 427 identifiable proteins after pooling all 6 samples. We cross-referenced these identified proteins with MitoCarta2.0, maintained by MIT's Broad Institute, a database of thoroughly vetted proteins that co-purify with mitochondria[8,10].

Using this approach, we were able to stratify our proteins into three groups of proteins based on evidence of mitochondrial localization (Figure 8A, B), 210 canonical mitochondrial proteins based on MitoCarta data from proteomics, computation, and microscopy analysis, 154 non-canonical mitochondrial proteins in the MitoCarta database that correlate with less pure mitochondrial fractions, and 63 proteins that are likely non-mitochondrial and do not show up in the MitoCarta database. Of course some of these "non-mitochondrial" proteins may still be mitochondrial as the MitoCarta data was not compiled from the visual system, where there could be uniquely-localized mitochondrial proteins.

After filtering for this external validation of mitochondrial association, we looked for the subset of proteins with predicted RNA binding potential by filtering proteins through David[63], Panther[64], and Uniport[65] data bases using the gene ontology term RNA binding. Proteins that met these criteria were then cross-referencing against datasets from the RNA-protein interactome of cardiac cells[66], HEK cells[67], and HeLa cells[68], as well as RNA binding protein databases AtTRACT and RBPDB[69-72]. This yielded the identification of 71 proteins with RNA binding properties, of which 43 had published evidence of direct interaction with mitochondria(Figure 8C, D). These included proteins with roles in translation, RNA processing, and RNA shuttling.

Since these data suggested that nuclear-encoded RNA binding proteins associate with mitochondria, we then asked whether there was also evidence for an association of nuclear-encoded mRNA on purified mitochondria. We purified mitochondria as above, extracted total RNA from pellets, and assayed for the presence of mRNA by qRT-PCR arrays. This identified a range of nuclear-encoded mitochondrial mRNAs, including genes that regulate mitochondrial

dynamics, cell death, and energetics (Figure 9A,B). All detected mRNAs amplified in less than 30 cycles, lending confidence to the integrity of these measurements.

To directly test the potential for mRNA tethering to outer mitochondrial membranes by RNA binding proteins, as implied by the OPP imaging experiments, mass spectrometry, and qRT-PCR array data, we treated mitochondrial isolates with Proteinase K to release surface proteins and associated mRNA, and then pelleted treated mitochondria to assay by qPCR for mRNAs released in the supernatant fractions (Figure 10A). As in Figure 8, to ensure that mRNAs detected in these assays were specific to mitochondria, we also verified the relative purity of mitochondrial fractions by western blotting for the presence of cytoplasmic contaminants, using actin an additional control (Figure 10B). We also took measures to verify that Proteinase K treatment did not release proteins from the interior of mitochondria, as shown by western blots against Complex III-Core Protein 2 and Complex V alpha subunit proteins (Figure 10C). In addition, there was no significant decrease in mitochondrial encoded mRNA ND4 in mitochondrial pellets and no significant increase in supernatant fractions (Figure 10D), providing strong evidence that Proteinase K did not interfere with inner mitochondrial protein or RNA. However, when purified mitochondria were tested for the release of nuclear-encoded mRNAs by Proteinase K, we found a significant number of mRNAs were released from mitochondrial pellets into the corresponding supernatant fraction, as compared to controls (Figure 10D). These mRNAs coded for proteins known to regulate mitochondrial dynamics, biogenesis, energetics, and RNA transport. We also found mRNA encoding cytoplasmic proteins GAPDH and actin bound to mitochondria, suggesting that bound mRNAs are not limited to those coding for mitochondrial-specific proteins. Interestingly, when we pre-treated in vivo with TTX at P11 and P13 and then assayed purified retinal mitochondrial transcripts from P15 mice,

298 there were essentially no significant changes in mitochondrial localized mRNAs dependent on
299 activity, although this could reflect an under sampling error as RGCs make up less than 1% of
300 retinal cells. Overall, these data indicate that mitochondria bind nuclear-encoded mRNAs known
301 to modulate mitochondrial size, number, and energetics, and that this process is mediated by RNA
302 binding proteins present on mitochondrial membranes.
303
304 **Discussion**
305 Proper CNS neuron development and homeostasis depends critically on mitochondrial
306 organization and function throughout distal axonal segments. Furthermore, mitochondria have to
307 be capable of dynamically changing to meet intra-axonal demands distal to the cell body. As result,
308 neurons and their distal segments have particularly demanding requirements for the active
309 expression, trafficking, and assembly of nuclear-encoded-mitochondrial-macromolecules
310 (proteins and mRNAs). Here we build upon the known mechanisms regulating rapid mitochondrial
311 change in axons, and present new findings in which mitochondria size, number, and total area are
312 regulated via activity and BDNF, and implicate a role for associated activity-regulated
313 mitochondrial localized translation in regulating distal mitochondrial dynamics in CNS axons.
314
315 <u>Activity and BDNF regulate mitochondrial morphology and localization</u>
316 Concomitant with eye opening, the visual system experiences increases in RGC electrical activity
317 and BDNF expression, triggered by Ca^{+2} signaling and the activation of CREB-mediated
318 transcription[52,73-75]. Both activity and BDNF signaling play a pivotal role in axon development,
319 including axon growth and presynaptic maturation, with mitochondrial dynamics and energetics
320 having stereotyped roles in these developmental events (reviewed elsewhere[76]). Yet, the link

between activity or BDNF signaling and changes in mitochondrial dynamics during CNS axon maturation in vivo had not been investigated. Here we show that RGC activity and downstream BDNF during eye opening is sufficient and necessary to increase mitochondrial size and number in RGCs' optic nerve axons during development, and that activity also plays a similar, albeit more muted role, in regulating mitochondrial morphology in RGCs' retinal axon segments. Whether this dependence is also observed during earlier periods of RGC development, e.g. when RGCs experience correlated waves of activity generated by amacrine cells before eye opening, or in other developing neurons, will be important questions to pursue.

In addition, we provide data supporting a new model in which activity and BDNF are modulating mitochondrial dynamics, biogenesis, and energetics in part through gene expression and local protein translation. Analysis of gene expression data pointed to the activation of transcriptional networks linked to PGC1-α and RICTOR by activity and BDNF during the period of eye opening, similar to findings in other neurons[77]. Furthermore, cellular energetics are linked to PGC1-α[78] and RICTOR[79] signaling, and our data reflected these findings[80], and suggest that activity and BDNF also regulate basal respiration in RGCs, with BDNF increasing the maximum respiration capacity of RGCs regardless of activity inhibition. Thus, our data is indicative of a generalized increase in mitochondrial biogenesis activity in RGCs treated with BDNF (and vice versa with TTX treatment), a mechanism by which morphology and distribution along axons may be regulated. Overall, these data also support a pathway in which eye opening and subsequent increased neuronal firing signal to modulate the expression of mitochondrial related transcription, mitochondrial dynamics, and energetics. There may also be a direct protein-based signaling cascade triggered by activity and subsequent BDNF signaling onto mitochondria, since there is

evidence that activity and BDNF increase respiration independent of nuclei in mitochondria-containing synaptosomal preparations[53,81,82].

Activity regulates a novel mechanism of mitochondrial localized translation

Axon segments can be up to a meter away from a neuron's cell body and nucleus, presenting a challenge for signaling and subsequent renewal of proteins required for normal neuronal function. Axonal transport of nuclear-encoded proteins, in which nuclear proteins are translated in the perinuclear space and transported down axons at rates of up to 8 mm/day for soluble proteins (i.e. metabolic enzymes) or 100 and even 400 mm/day when associated with mitochondria or neuropeptide containing vesicles, respectively[59,83,84], may not be quick enough to resupply distal axonal sites at times of rapid demand. In addition, nuclear-encoded mRNAs including some for mitochondrial proteins[24-26] are transported to distal axon sites including in RGC axons in the mouse[27], ready to be translated locally and on demand[23], suggesting that mitochondria function is in part maintained by active axonal localized translation. Consistent with our findings, activity modulation and neurotrophic factors including BDNF regulate local translation in xenopus neurons[85,86] and our extend this model showing that such translation occurs at mitochondria in an activity-dependent manner. The enrichment in mRNAs encoding mitochondrial proteins on or near mitochondria[28-32] and the finding that ribosomes can directly bind to mitochondria membranes via TOM proteins and act in co-translation protein import in yeast[33-35], together suggest a novel mechanism whereby increased neuronal firing and BDNF downstream signaling pathways directly regulate mitochondrial dynamics through modified local translation (Figure 12). This model will require additional molecular investigation in mammalian axons, such as the development of approaches to inhibit protein synthesis in specific subcellular compartments.

Implications for aging and disease

These data move towards identifying mechanisms regulating mitochondrial organization and nuclear-encoded mitochondrial transcript localization in CNS axons during normal developmental, but raise questions to what degree similar mechanisms act in aging or neurodegenerative disease. Declining or defective mitochondrial function has been linked to many neurodegenerative diseases[87]. In humans and in mammalian animal models, defective axonal mRNA transport mechanisms have been implicated in the pathogenesis of neuropathies including spinal muscle atrophy, amyotrophic lateral sclerosis, and distal hereditary neuropathy[88-90], and declining metabolic function is increasingly linked to reduced expression of mitochondrial transcripts[91,92]. Thus, understanding how the expression and local translation of nuclear mitochondrial transcripts are regulated and how these influence mitochondrial function may yield new approaches to treat dysfunction in the nervous system.

Materials and Methods

Animal use statement. Experiments conformed to the ARVO Statement for the Use of Animals in Ophthalmic and Vision Research and were approved by the Stanford University Biosafety Committee and the Institutional Animal Care and Use Committee. Strains used in these experiments included wild type CD-1, C57BL/6, and B6.Cg-Tg(Thy1-CFP/COX8A)S2Lich/J mice (The Jackson Laboratory).

Cell Culture. RGCs were purified from male and female postnatal day 1/2 (P1/2) C57BL/6 mice (Charles River Laboratories) by immunopanning, and cultured on poly-D-lysine- (10 μg/mL;

Sigma Aldrich, P-6407) and laminin-coated (2 µg/mL; Sigma, L-6274) cover glass bottom 96 well plates (Greiner Bio-One)[93,94], in media with or without BDNF supplement as previously described[86]. Then, RGCs were treated with baculoviruses to label mitochondria (BacMam 2.0, Thermo Fisher Scientific, C10601) and 48 hrs later incubated with pharmacological agents, at stated concentrations and times. In RNA or protein labeling experiments RGCs were incubated with EU for 2 hrs or OPP for 15 min (according to the Click-iT Nascent RNA or Protein Synthesis Assay Kit from Thermo Fisher Scientific, C10327 or C10456). After all incubations cells were then fixated (4% PFA PBS), permeabilizated (0.5% Triton PBS), and in EU- or OPP-incubated cells, Click labeling reaction were performed. To identify ribosomes, cells were incubated with antibodies against ribosomal protein S3 (Cell Signaling Technology, D50G7) at 1:100 overnight at 4°C, and secondary Alexa-647 conjugated antibodies at 1:500 for 2hrs at room temperature. To label growth cones, cells were incubated with Alexa Fluor® 647 Phalloidin (Thermo Fisher Scientific, A22287) at 1:40 room temp. for 30 min prior to confocal imaging. In oxygen consumption experiments, RGCs were plated as described above, with or without BDNF, at 40k/well in 96 well plates designed for the Seahorse XF96 instrument (Agilent, 101085-004). After culturing for 24hrs, media was exchanged with Assay Media (Agilent, 102365-100) and FluxPak injectable ports were loaded with drugs as recommended by mitochondrial stress test kit (Agilent, 103015-100). TTX was loaded in the empty port A as the first injection, followed by Oligomycin, FCCP, and Rotenone/Antimycin A, respectively. After assay was complete oxygen consumption values were normalized to the number of Dapi positive cells per well.

Imaging. B6.Cg-Tg(Thy1-CFP/COX8A)S2Lich/J mice (CFP/COX8a, Jackson labs) were euthanized and perfused with 4% PFA in PBS at P9, P13, P15, and P45. Perfused animals were

413 then enucleated and the eyes and the optic nerves post-fixed in 4% PFA for 1-3 hours. Post fixed
414 tissues were whole mounted on slides in Vecta-Shield mounting medium (Vector Labs, #H-1400)
415 and imaged on a Zeiss LSM 710 confocal microscope. Compressed Z-stacks were analyzed by
416 selecting nine random 25 x 50 µm sections and then measuring CFP expression with the ImageJ
417 particle analyzer tool (National Institutes of Health). All images of cultured RGCs were collected
418 on a Zeiss LSM 880 confocal system with a 40x/63x objective and using airyscan imaging mode,
419 followed by airyscan processing using Zen software. Mitochondrial size, translation spot size, and
420 colocalization analysis was conducted using Volocity Imaging Software (Perkin Elmer).
421
422 **Electron microscopy.** Adult CD-1 mice under anesthesia were perfused with one half
423 Karnovsky's fixative; 2.5% glutaraldehyde and 2% paraformaldehyde (PFA) in 0.2M cacodylate
424 buffer. Mice were euthanized and eyes with optic nerves were post fixed in half Karnovsky's
425 fixative. Tissues were placed in 2% glutaraldehyde overnight and then rinsed in 0.1M phosphate
426 buffer with osmium tetraoxide. Osmicated tissues were rinsed in 0.15M phosphate buffer and
427 dehydrated with graded concentrations of cold ethanol, ranging from 25 to 100%. Dehydrated
428 tissues were rinsed with propylene oxide and embedded in Epon-Araldite with DMP-30 (All
429 reagents were purchased from Electron Microscopy Sciences). Mitochondrial numbers were
430 counted per axon area delineated by morphological features. Mitochondrial and axon boundaries
431 were manually traced, and the areas were calculated using ImageJ analysis software (National
432 Institutes of Health).
433
434 **Mitochondrial Purification.** Whole retinas or optic nerves and tracts were quickly dissected from
435 CO2 sacrificed mice, and homogenized using a dounce tissue grinder (Wheaton, 357538) with 20-

436 30 strokes in mitochondrial isolation buffer (provided in the Mitochondria Isolation Kit, Miltenyi
437 Biotec, 130-096-946) with protease inhibitors (Thermofisher Scientific, 78425). The homogenate
438 was then spun at 1000g and the supernatant was removed for subsequent magnet based
439 mitochondrial isolation according to Milteny Biotec's Mitochondrial Isolation Kit. Isolated
440 mitochondria were washed and re-pelleted three times to insure mitochondrial fractions were pure
441 and intact, for all downstream experiments. In addition, all procedures were performed on ice or
442 at 4°C, to preserve mitochondrial integrity.
443
444 **FACS analyses of mitochondria.** CFP-expressing mitochondria were analyzed with forward and
445 side scatter in a Becton Dickinson FACScan (Becton Dickinson, San Jose, CA). Data were
446 acquired in list mode, evaluated with WinList software (Verity Software House). In some
447 experiments, mitochondria were detected with anti-TOM20 antibodies (Abcam, ab78547) or
448 mitotracker CMXROS (Thermofisher Scientific, M7512). To determine if mitochondria were
449 intact and viable, FACS sorted mitochondria were equilibrated with the membrane potential–
450 sensitive dye JC-1 (500 nM; 5,5'6,6-tetra-chloro-1,1,3,3-tetraethylbenzimidazol-carbocyanine
451 iodide; Thermofisher Scientific, T3168) for 20 minutes with or without FCCP (10 μM;
452 carbonylcyanide-P-trifluoromethoxyphenylhydrazone; Sigma Aldrich, C2920).
453
454 **Western Blots.** To further evaluate the structural integrity and purity of isolated mitochondria,
455 mitochondria were analyzed by western blot using the following antibodies. Antibodies against
456 inner and outer mitochondrial membrane integrity proteins include; Outer Membrane - Porin
457 (VDAC1), Inner Membrane - Ubiquinol Cytochrome C Reductase Core Protein I, Intermembrane
458 Space - Cytochrome C and Complex Va, and Matrix Space-Cyclophilin 40, (Abcam-ab110414;

459 ab14734, ab110252, ab110325, ab110273, and ab110324). Electron transport chain protein
460 antibodies include; Complex I subunit (NDUFB8), Complex II-30kDa (SH3B), Complex III-Core
461 Protein 2 (UQCRC2), Complex IV subunit I (MTCO1), and Complex V alpha subunit (ATP5A)
462 (Abcam-ab1104; ab110242, ab14714, ab14745, ab14705, and ab14748). Cytoplasmic antibodies
463 include; GAPDH and β-Actin (Cell Signaling Technology, 2118S and 8457). GFP/CFP antibodies
464 (Thermofisher Scientific, A10262) were used as controls for the integrity of mitochondrial
465 fractions collected from Thy1-CFP/COX8A mice.
466
467 **Proteomics.** To detect mitochondrial associated proteins, mitochondrial purification was
468 performed on 24 optic nerves and 6 retinas. Resulting mitochondrial pellets were solubilized with
469 5% rapigest in TNE buffer and then boiled for 5 min, followed by reduction in 1mM Tris(2-
470 carboxyethyl)phosphine hydrochloride at 37℃ for 30min. Then samples were alkylated in .5mM
471 2-iodoacetamide at 37℃ for 30min, followed by trypsin digestions at 1:50 (enzyme:protein)
472 overnight at 37℃ and the addition of 250mM HCl at 37℃ for 1hr. Samples were then centrifuged
473 and peptides were extracted from the supernatant and desalted using Aspire RP30 desalting
474 columns (Thermo Scientific)[95]. Trypsin-digested peptides were analyzed by LC-MS/MS[96] on the
475 TripleTOF™ 5600 hybrid mass spectrometer (ABSCIEX). MS/MS data were acquired in a data-
476 dependent manner in which the MS1 data was acquired for 250 ms at m/z of 400 to 1250 Da and
477 the MS/MS data was acquired from m/z of 50 to 2,000 Da. For Independent data acquisition (IDA)
478 parameters MS1-TOF 250 milliseconds, followed by 50 MS2 events of 25 milliseconds each. The
479 IDA criteria; over 200 counts threshold, charge state of plus 2-4 with 4 seconds exclusion window.
480 Finally, the collected data were analyzed and normalized[97] using MASCOT® (Matrix Sciences)
481 and Protein Pilot 4.0 (ABSCIEX) for peptide identifications normalized based on spectral

abundance factors.

RNA detection. To detect mitochondrial or nuclear-encoded mRNA transcripts, RNA was extracted from isolated RGCs or mitochondria from retina or optic nerve and tract using the RNeasy Plus Micro Kit (Qiagen, 74034). RNA isolates were then processed for RT² Profiler™ PCR Arrays (Mouse Mitochondrial and Mitochondria Energy Metabolism, PAMM-087ZE and PAMM-008ZE). For mitochondrial RNA release assays, isolated mitochondria were resuspended in mitochondrial suspension buffer (provided in Mitochondria Isolation Kit) and incubated with Proteinase K (Thermofisher Scientific, 25530049) at 5ug/mL for 10 min. Mitochondria were then pelleted, and supernatant and mitochondrial pellets were separately processed for RNA purification and subsequent qPCR arrays. All qPCR data were acquired on QuantStudio 7 Flex Real-Time PCR System (Applied Biosystems, Thermofisher Scientific).

Pharmacologic interventions. Mice were anesthetized with xylazine (10 mg/kg, IP) and ketamine (80 mg/kg, IP). Anesthetized mice were injected intravitreally (1-2 µl) with vehicle, Hank's balanced salt solution (HBS, Invitrogen), BDNF (3µg/µl; Peprotech #450-02), tetrodotoxin (TTX; 3 µM, Sigma #T8024), or combined TTX (3 µM) and BDNF (3.3 µg/µl; Peprotech).

Eyelid opening or suturing. For premature eyelid opening experiments, P10 mice were anesthetized as above and eyelids were gently pried open with forceps as described[98]. Eyes were then treated with sterile 2.5% hydroxypropyl methylcellulose (Goniosol, Akorn) every 12-18 hours to ensure eyes remained open and lubricated throughout the duration of the experiment. For extended eyelid closure experiments, P11 pups were anesthetized and two mattress sutures were

placed along the eyelid margin to prevent eye opening as described [99]. Animals were checked daily to ensure sutured eyes remained closed until euthanasia.

Graphing and Statistics. Data presentation and statistical analysis was done in Prism (Graphpad). To compare quantitative variables, Student's t-tests or ANOVA with post-hoc t-tests were done with a p-value < 0.05 indicating statistical significance.

Acknowledgements

We gratefully acknowledge funding from the NIH R01-EY020913 (JLG), P30-EY014801 (University of Miami), P30-EY026877 (Stanford University), F31-NS087789 (AK), as well as unrestricted grants from Research to Prevent Blindness, Inc. We thank the following for their technical support; Peggy Bates for electron microscopy, George McNamara and Gabe Gaidosh for microscopy, Kristina Russano and Eleut Hernandez for animal husbandry, Oliver Umland for assistance in flow cytometry, and Majid Ghassemian for mass spectrometry support.

Competing interests: The authors declare that no competing interests exist.

References

1 Wong-Riley, M. T. Energy metabolism of the visual system. *Eye Brain* **2**, 99-116, doi:10.2147/EB.S9078 (2010).

2 Agathocleous, M. *et al.* Metabolic differentiation in the embryonic retina. *Nat Cell Biol* **14**, 859-864, doi:10.1038/ncb2531 (2012).

3 Agostini, M. *et al.* Metabolic reprogramming during neuronal differentiation. *Cell Death Differ* **23**, 1502-1514, doi:10.1038/cdd.2016.36 (2016).

4 Kann, O. & Kovacs, R. Mitochondria and neuronal activity. *American journal of physiology. Cell physiology* **292**, C641-657, doi:10.1152/ajpcell.00222.2006 (2007).

5 Johnson, D. T. *et al.* Tissue heterogeneity of the mammalian mitochondrial proteome. *American journal of physiology. Cell physiology* **292**, C689-697, doi:10.1152/ajpcell.00108.2006 (2007).

6 Gaston, D., Tsaousis, A. D. & Roger, A. J. Predicting proteomes of mitochondria and related organelles from genomic and expressed sequence tag data. *Methods Enzymol* **457**, 21-47, doi:10.1016/S0076-6879(09)05002-2 (2009).

7 Mootha, V. K. *et al.* Integrated analysis of protein composition, tissue diversity, and gene regulation in mouse mitochondria. *Cell* **115**, 629-640 (2003).

8 Pagliarini, D. J. *et al.* A mitochondrial protein compendium elucidates complex I disease biology. *Cell* **134**, 112-123, doi:10.1016/j.cell.2008.06.016 (2008).

9 Sickmann, A. *et al.* The proteome of Saccharomyces cerevisiae mitochondria. *Proc Natl Acad Sci U S A* **100**, 13207-13212, doi:10.1073/pnas.2135385100 (2003).

10 Calvo, S. E., Clauser, K. R. & Mootha, V. K. MitoCarta2.0: an updated inventory of mammalian mitochondrial proteins. *Nucleic Acids Res* **44**, D1251-1257, doi:10.1093/nar/gkv1003 (2016).

11 Anderson, S. *et al.* Sequence and organization of the human mitochondrial genome. *Nature* **290**, 457-465 (1981).

12 Kurland, C. G. & Andersson, S. G. Origin and evolution of the mitochondrial proteome. *Microbiology and molecular biology reviews : MMBR* **64**, 786-820 (2000).

13 Zhou, B. *et al.* Facilitation of axon regeneration by enhancing mitochondrial transport and rescuing energy deficits. *J Cell Biol* **214**, 103-119, doi:10.1083/jcb.201605101 (2016).

14 Ryan, M. T. & Hoogenraad, N. J. Mitochondrial-nuclear communications. *Annu Rev Biochem* **76**, 701-722, doi:10.1146/annurev.biochem.76.052305.091720 (2007).

15 Varadi, A. *et al.* Cytoplasmic dynein regulates the subcellular distribution of mitochondria by controlling the recruitment of the fission factor dynamin-related protein-1. *J Cell Sci* **117**, 4389-4400, doi:10.1242/jcs.01299 (2004).

16 Hancock, W. O. Bidirectional cargo transport: moving beyond tug of war. *Nat Rev Mol Cell Biol* **15**, 615-628, doi:10.1038/nrm3853 (2014).

17 Stuart, R. A., Cyr, D. M., Craig, E. A. & Neupert, W. Mitochondrial molecular chaperones: their role in protein translocation. *Trends Biochem Sci* **19**, 87-92, doi:10.1016/0968-0004(94)90041-8 (1994).

18 Sheng, Z. H. & Cai, Q. Mitochondrial transport in neurons: impact on synaptic homeostasis and neurodegeneration. *Nat Rev Neurosci* **13**, 77-93, doi:10.1038/nrn3156 (2012).

19 Youle, R. J. & van der Bliek, A. M. Mitochondrial fission, fusion, and stress. *Science* **337**, 1062-1065, doi:10.1126/science.1219855 (2012).

20 Amiri, M. & Hollenbeck, P. J. Mitochondrial biogenesis in the axons of vertebrate peripheral neurons. *Dev Neurobiol* **68**, 1348-1361, doi:10.1002/dneu.20668 (2008).

21 Mattson, M. P., Gleichmann, M. & Cheng, A. Mitochondria in neuroplasticity and neurological disorders. *Neuron* **60**, 748-766, doi:10.1016/j.neuron.2008.10.010 (2008).

22 Van Laar, V. S. *et al.* Evidence for compartmentalized axonal mitochondrial biogenesis: Mitochondrial DNA replication increases in distal axons as an early response to Parkinson's disease-relevant stress. *J Neurosci*, doi:10.1523/JNEUROSCI.0541-18.2018 (2018).

574 23 Jung, H., Yoon, B. C. & Holt, C. E. Axonal mRNA localization and local protein synthesis
575 in nervous system assembly, maintenance and repair. *Nat Rev Neurosci* **13**, 308-324,
576 doi:10.1038/nrn3210 (2012).
577 24 Gioio, A. E. *et al.* Local synthesis of nuclear-encoded mitochondrial proteins in the
578 presynaptic nerve terminal. *Journal of neuroscience research* **64**, 447-453 (2001).
579 25 Aschrafi, A., Natera-Naranjo, O., Gioio, A. E. & Kaplan, B. B. Regulation of axonal
580 trafficking of cytochrome c oxidase IV mRNA. *Mol Cell Neurosci* **43**, 422-430,
581 doi:10.1016/j.mcn.2010.01.009 (2010).
582 26 Hillefors, M., Gioio, A. E., Mameza, M. G. & Kaplan, B. B. Axon viability and
583 mitochondrial function are dependent on local protein synthesis in sympathetic neurons.
584 *Cell Mol Neurobiol* **27**, 701-716, doi:10.1007/s10571-007-9148-y (2007).
585 27 Shigeoka, T. *et al.* Dynamic Axonal Translation in Developing and Mature Visual Circuits.
586 *Cell* **166**, 181-192, doi:10.1016/j.cell.2016.05.029 (2016).
587 28 Mercer, T. R. *et al.* The human mitochondrial transcriptome. *Cell* **146**, 645-658,
588 doi:10.1016/j.cell.2011.06.051 (2011).
589 29 Gehrke, S. *et al.* PINK1 and Parkin control localized translation of respiratory chain
590 component mRNAs on mitochondria outer membrane. *Cell Metab* **21**, 95-108,
591 doi:10.1016/j.cmet.2014.12.007 (2015).
592 30 Matsumoto, S. *et al.* Localization of mRNAs encoding human mitochondrial oxidative
593 phosphorylation proteins. *Mitochondrion* **12**, 391-398, doi:10.1016/j.mito.2012.02.004
594 (2012).
595 31 Wong, H. H. *et al.* RNA Docking and Local Translation Regulate Site-Specific Axon
596 Remodeling In Vivo. *Neuron* **95**, 852-868 e858, doi:10.1016/j.neuron.2017.07.016 (2017).

32 Kaewsapsak, P., Shechner, D. M., Mallard, W., Rinn, J. L. & Ting, A. Y. Live-cell mapping of organelle-associated RNAs via proximity biotinylation combined with protein-RNA crosslinking. *Elife* **6**, doi:10.7554/eLife.29224 (2017).

33 Kellems, R. E., Allison, V. F. & Butow, R. A. Cytoplasmic type 80S ribosomes associated with yeast mitochondria. IV. Attachment of ribosomes to the outer membrane of isolated mitochondria. *J Cell Biol* **65**, 1-14 (1975).

34 Crowley, K. S. & Payne, R. M. Ribosome binding to mitochondria is regulated by GTP and the transit peptide. *J Biol Chem* **273**, 17278-17285 (1998).

35 Williams, C. C., Jan, C. H. & Weissman, J. S. Targeting and plasticity of mitochondrial proteins revealed by proximity-specific ribosome profiling. *Science* **346**, 748-751, doi:10.1126/science.1257522 (2014).

36 Majdan, M. & Shatz, C. J. Effects of visual experience on activity-dependent gene regulation in cortex. *Nat Neurosci* **9**, 650-659, doi:10.1038/nn1674 (2006).

37 Tian, N. & Copenhagen, D. R. Visual stimulation is required for refinement of ON and OFF pathways in postnatal retina. *Neuron* **39**, 85-96 (2003).

38 Feller, M. B. Retinal waves are likely to instruct the formation of eye-specific retinogeniculate projections. *Neural development* **4**, 24, doi:10.1186/1749-8104-4-24 (2009).

39 Reese, B. E. Development of the retina and optic pathway. *Vision research* **51**, 613-632, doi:10.1016/j.visres.2010.07.010 (2011).

40 Chandrasekaran, A. R., Plas, D. T., Gonzalez, E. & Crair, M. C. Evidence for an instructive role of retinal activity in retinotopic map refinement in the superior colliculus of the mouse. *J Neurosci* **25**, 6929-6938, doi:10.1523/JNEUROSCI.1470-05.2005 (2005).

620 41 Feller, M. B., Wellis, D. P., Stellwagen, D., Werblin, F. S. & Shatz, C. J. Requirement for
621 cholinergic synaptic transmission in the propagation of spontaneous retinal waves. *Science*
622 **272**, 1182-1187 (1996).
623 42 Akerman, C. J., Smyth, D. & Thompson, I. D. Visual experience before eye-opening and
624 the development of the retinogeniculate pathway. *Neuron* **36**, 869-879 (2002).
625 43 Huberman, A. D. *et al.* Eye-specific retinogeniculate segregation independent of normal
626 neuronal activity. *Science* **300**, 994-998, doi:10.1126/science.1080694 (2003).
627 44 Etxeberria, A. *et al.* Dynamic Modulation of Myelination in Response to Visual Stimuli
628 Alters Optic Nerve Conduction Velocity. *J Neurosci* **36**, 6937-6948,
629 doi:10.1523/JNEUROSCI.0908-16.2016 (2016).
630 45 Young, R. W. Cell death during differentiation of the retina in the mouse. *J Comp Neurol*
631 **229**, 362-373, doi:10.1002/cne.902290307 (1984).
632 46 Galli-Resta, L. & Ensini, M. An intrinsic time limit between genesis and death of individual
633 neurons in the developing retinal ganglion cell layer. *J Neurosci* **16**, 2318-2324 (1996).
634 47 Beros, J., Rodger, J. & Harvey, A. R. Developmental retinal ganglion cell death and
635 retinotopicity of the murine retinocollicular projection. *Dev Neurobiol*,
636 doi:10.1002/dneu.22559 (2017).
637 48 Frank, S. *et al.* The role of dynamin-related protein 1, a mediator of mitochondrial fission,
638 in apoptosis. *Developmental cell* **1**, 515-525 (2001).
639 49 Estaquier, J. & Arnoult, D. Inhibiting Drp1-mediated mitochondrial fission selectively
640 prevents the release of cytochrome c during apoptosis. *Cell Death Differ* **14**, 1086-1094,
641 doi:10.1038/sj.cdd.4402107 (2007).

50 Liu, C. J., Chaturvedi, N., Barnstable, C. J. & Dreyer, E. B. Retinal Thy-1 expression during development. *Invest Ophthalmol Vis Sci* **37**, 1469-1473 (1996).

51 Mojumder, D. K., Sherry, D. M. & Frishman, L. J. Contribution of voltage-gated sodium channels to the b-wave of the mammalian flash electroretinogram. *The Journal of physiology* **586**, 2551-2580, doi:10.1113/jphysiol.2008.150755 (2008).

52 Seki, M., Nawa, H., Fukuchi, T., Abe, H. & Takei, N. BDNF is upregulated by postnatal development and visual experience: quantitative and immunohistochemical analyses of BDNF in the rat retina. *Investigative ophthalmology & visual science* **44**, 3211-3218 (2003).

53 Markham, A., Cameron, I., Franklin, P. & Spedding, M. BDNF increases rat brain mitochondrial respiratory coupling at complex I, but not complex II. *Eur J Neurosci* **20**, 1189-1196, doi:10.1111/j.1460-9568.2004.03578.x (2004).

54 Su, B., Ji, Y. S., Sun, X. L., Liu, X. H. & Chen, Z. Y. Brain-derived neurotrophic factor (BDNF)-induced mitochondrial motility arrest and presynaptic docking contribute to BDNF-enhanced synaptic transmission. *J Biol Chem* **289**, 1213-1226, doi:10.1074/jbc.M113.526129 (2014).

55 Guo, J. *et al.* BDNF pro-peptide regulates dendritic spines via caspase-3. *Cell Death Dis* **7**, e2264, doi:10.1038/cddis.2016.166 (2016).

56 Jao, C. Y. & Salic, A. Exploring RNA transcription and turnover in vivo by using click chemistry. *Proc Natl Acad Sci U S A* **105**, 15779-15784, doi:10.1073/pnas.0808480105 (2008).

663 57 Liu, J., Xu, Y., Stoleru, D. & Salic, A. Imaging protein synthesis in cells and tissues with
664 an alkyne analog of puromycin. *Proc Natl Acad Sci U S A* **109**, 413-418,
665 doi:10.1073/pnas.1111561108 (2012).
666 58 Lipton, S. A. Blockade of electrical activity promotes the death of mammalian retinal
667 ganglion cells in culture. *Proc Natl Acad Sci U S A* **83**, 9774-9778 (1986).
668 59 Griffin, J. W., Price, D. L., Drachman, D. B. & Engel, W. K. Axonal transport to and from
669 the motor nerve ending. *Ann N Y Acad Sci* **274**, 31-45 (1976).
670 60 Goldberg, J. L., Klassen, M. P., Hua, Y. & Barres, B. A. Amacrine-signaled loss of intrinsic
671 axon growth ability by retinal ganglion cells. *Science* **296**, 1860-1864,
672 doi:10.1126/science.1068428 (2002).
673 61 Graifer, D., Malygin, A., Zharkov, D. O. & Karpova, G. Eukaryotic ribosomal protein S3:
674 A constituent of translational machinery and an extraribosomal player in various cellular
675 processes. *Biochimie* **99**, 8-18, doi:10.1016/j.biochi.2013.11.001 (2014).
676 62 Franko, A. *et al.* Efficient isolation of pure and functional mitochondria from mouse tissues
677 using automated tissue disruption and enrichment with anti-TOM22 magnetic beads. *PLoS*
678 *One* **8**, e82392, doi:10.1371/journal.pone.0082392 (2013).
679 63 Huang da, W., Sherman, B. T. & Lempicki, R. A. Systematic and integrative analysis of
680 large gene lists using DAVID bioinformatics resources. *Nat Protoc* **4**, 44-57,
681 doi:10.1038/nprot.2008.211 (2009).
682 64 Thomas, P. D. *et al.* PANTHER: a library of protein families and subfamilies indexed by
683 function. *Genome Res* **13**, 2129-2141, doi:10.1101/gr.772403 (2003).

684 65 Pundir, S., Magrane, M., Martin, M. J., O'Donovan, C. & UniProt, C. Searching and
685 Navigating UniProt Databases. *Curr Protoc Bioinformatics* **50**, 1 27 21-10,
686 doi:10.1002/0471250953.bi0127s50 (2015).
687 66 Liao, Y. *et al.* The Cardiomyocyte RNA-Binding Proteome: Links to Intermediary
688 Metabolism and Heart Disease. *Cell Rep* **16**, 1456-1469, doi:10.1016/j.celrep.2016.06.084
689 (2016).
690 67 Baltz, A. G. *et al.* The mRNA-bound proteome and its global occupancy profile on protein-
691 coding transcripts. *Mol Cell* **46**, 674-690, doi:10.1016/j.molcel.2012.05.021 (2012).
692 68 Castello, A. *et al.* Insights into RNA biology from an atlas of mammalian mRNA-binding
693 proteins. *Cell* **149**, 1393-1406, doi:10.1016/j.cell.2012.04.031 (2012).
694 69 Giudice, G., Sanchez-Cabo, F., Torroja, C. & Lara-Pezzi, E. ATtRACT-a database of
695 RNA-binding proteins and associated motifs. *Database (Oxford)* **2016**,
696 doi:10.1093/database/baw035 (2016).
697 70 Cook, K. B., Kazan, H., Zuberi, K., Morris, Q. & Hughes, T. R. RBPDB: a database of
698 RNA-binding specificities. *Nucleic Acids Res* **39**, D301-308, doi:10.1093/nar/gkq1069
699 (2011).
700 71 Gerstberger, S., Hafner, M. & Tuschl, T. A census of human RNA-binding proteins. *Nat*
701 *Rev Genet* **15**, 829-845, doi:10.1038/nrg3813 (2014).
702 72 Castello, A. *et al.* Comprehensive Identification of RNA-Binding Domains in Human
703 Cells. *Mol Cell* **63**, 696-710, doi:10.1016/j.molcel.2016.06.029 (2016).
704 73 Shieh, P. B., Hu, S. C., Bobb, K., Timmusk, T. & Ghosh, A. Identification of a signaling
705 pathway involved in calcium regulation of BDNF expression. *Neuron* **20**, 727-740 (1998).

74 Lein, E. S., Hohn, A. & Shatz, C. J. Dynamic regulation of BDNF and NT-3 expression during visual system development. *The Journal of comparative neurology* **420**, 1-18 (2000).

75 Lu, B. BDNF and activity-dependent synaptic modulation. *Learning & memory* **10**, 86-98, doi:10.1101/lm.54603 (2003).

76 Marosi, K. & Mattson, M. P. BDNF mediates adaptive brain and body responses to energetic challenges. *Trends Endocrinol Metab* **25**, 89-98, doi:10.1016/j.tem.2013.10.006 (2014).

77 Camandola, S. & Mattson, M. P. Brain metabolism in health, aging, and neurodegeneration. *EMBO J* **36**, 1474-1492, doi:10.15252/embj.201695810 (2017).

78 Wareski, P. *et al.* PGC-1{alpha} and PGC-1{beta} regulate mitochondrial density in neurons. *J Biol Chem* **284**, 21379-21385, doi:10.1074/jbc.M109.018911 (2009).

79 Schieke, S. M. *et al.* The mammalian target of rapamycin (mTOR) pathway regulates mitochondrial oxygen consumption and oxidative capacity. *J Biol Chem* **281**, 27643-27652, doi:10.1074/jbc.M603536200 (2006).

80 Divakaruni, A. S., Paradyse, A., Ferrick, D. A., Murphy, A. N. & Jastroch, M. Analysis and interpretation of microplate-based oxygen consumption and pH data. *Methods Enzymol* **547**, 309-354, doi:10.1016/B978-0-12-801415-8.00016-3 (2014).

81 Burkhalter, J., Fiumelli, H., Allaman, I., Chatton, J. Y. & Martin, J. L. Brain-derived neurotrophic factor stimulates energy metabolism in developing cortical neurons. *J Neurosci* **23**, 8212-8220 (2003).

82 Chan, S. L. & Quastel, J. H. Tetrodotoxin: effects on brain metabolism in vitro. *Science* **156**, 1752-1753 (1967).

729 83 Smith, R. S. The short term accumulation of axonally transported organelles in the region
730 of localized lesions of single myelinated axons. *J Neurocytol* **9**, 39-65 (1980).
731 84 Tsukita, S. & Ishikawa, H. The movement of membranous organelles in axons. Electron
732 microscopic identification of anterogradely and retrogradely transported organelles. *J Cell*
733 *Biol* **84**, 513-530 (1980).
734 85 Yao, J., Sasaki, Y., Wen, Z., Bassell, G. J. & Zheng, J. Q. An essential role for beta-actin
735 mRNA localization and translation in Ca2+-dependent growth cone guidance. *Nat*
736 *Neurosci* **9**, 1265-1273, doi:10.1038/nn1773 (2006).
737 86 Leung, K. M. *et al.* Asymmetrical beta-actin mRNA translation in growth cones mediates
738 attractive turning to netrin-1. *Nat Neurosci* **9**, 1247-1256, doi:10.1038/nn1775 (2006).
739 87 Lin, M. T. & Beal, M. F. Mitochondrial dysfunction and oxidative stress in
740 neurodegenerative diseases. *Nature* **443**, 787-795, doi:10.1038/nature05292 (2006).
741 88 Alami, N. H. *et al.* Axonal transport of TDP-43 mRNA granules is impaired by ALS-
742 causing mutations. *Neuron* **81**, 536-543, doi:10.1016/j.neuron.2013.12.018 (2014).
743 89 Lemmens, R., Moore, M. J., Al-Chalabi, A., Brown, R. H., Jr. & Robberecht, W. RNA
744 metabolism and the pathogenesis of motor neuron diseases. *Trends Neurosci* **33**, 249-258,
745 doi:10.1016/j.tins.2010.02.003 (2010).
746 90 Rossor, A. M., Kalmar, B., Greensmith, L. & Reilly, M. M. The distal hereditary motor
747 neuropathies. *J Neurol Neurosurg Psychiatry* **83**, 6-14, doi:10.1136/jnnp-2011-300952
748 (2012).
749 91 Zahn, J. M. *et al.* AGEMAP: a gene expression database for aging in mice. *PLoS genetics*
750 **3**, e201, doi:10.1371/journal.pgen.0030201 (2007).

751 92 Blalock, E. M. *et al.* Gene microarrays in hippocampal aging: statistical profiling identifies
752 novel processes correlated with cognitive impairment. *J Neurosci* **23**, 3807-3819 (2003).
753 93 Steketee, M. B. *et al.* Mitochondrial dynamics regulate growth cone motility, guidance,
754 and neurite growth rate in perinatal retinal ganglion cells in vitro. *Invest Ophthalmol Vis*
755 *Sci* **53**, 7402-7411, doi:10.1167/iovs.12-10298 (2012).
756 94 Barres, B. A., Silverstein, B. E., Corey, D. P. & Chun, L. L. Immunological,
757 morphological, and electrophysiological variation among retinal ganglion cells purified by
758 panning. *Neuron* **1**, 791-803 (1988).
759 95 Guttman, M. *et al.* Interactions of the NPXY microdomains of the low density lipoprotein
760 receptor-related protein 1. *Proteomics* **9**, 5016-5028, doi:10.1002/pmic.200900457 (2009).
761 96 McCormack, A. L. *et al.* Direct analysis and identification of proteins in mixtures by
762 LC/MS/MS and database searching at the low-femtomole level. *Anal Chem* **69**, 767-776
763 (1997).
764 97 Paoletti, A. C. *et al.* Quantitative proteomic analysis of distinct mammalian Mediator
765 complexes using normalized spectral abundance factors. *Proc Natl Acad Sci U S A* **103**,
766 18928-18933, doi:10.1073/pnas.0606379103 (2006).
767 98 Watanabe, H., Tisdale, A. S. & Gipson, I. K. Eyelid opening induces expression of a
768 glycocalyx glycoprotein of rat ocular surface epithelium. *Investigative ophthalmology &*
769 *visual science* **34**, 327-338 (1993).
770 99 Gordon, J. A. & Stryker, M. P. Experience-dependent plasticity of binocular responses in
771 the primary visual cortex of the mouse. *The Journal of neuroscience : the official journal*
772 *of the Society for Neuroscience* **16**, 3274-3286 (1996).
773

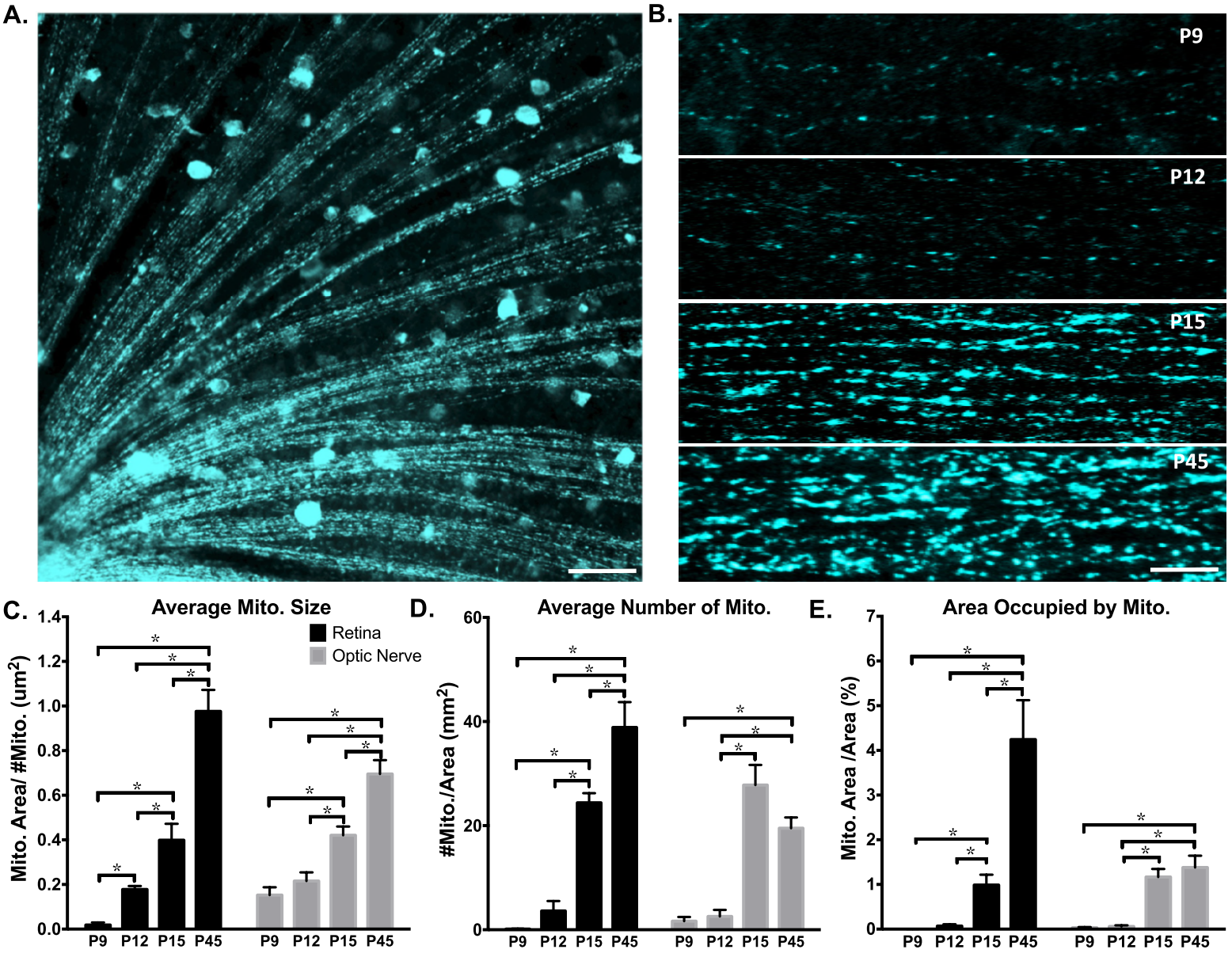

Figure 1. Axonal mitochondria increase in size, number and area through eye development. CFP+ mitochondria were imaged by confocal microscopy and analyzed in ImageJ. (A) Example image of mitochondrial labeling within retinal RGC axon segments (50um scale bar) and (B) in optic nerve RGC axon segments from postnatal day 9 (P9), P12, P15, and P45 mice (1um scale bar). (C-E) In both retinal and optic nerve RGC axons, the average mitochondrial size, number, and area (measured as percent of cross sections, representing fractional volume) increased from P9 to adulthood. (Error bars indicate SEM; N≥ 3 mice per age, with 9 images analyzed per animal; one-way ANOVA with Holm-Sidak correction for multiple comparisons, * $p \leq 0.05$.)

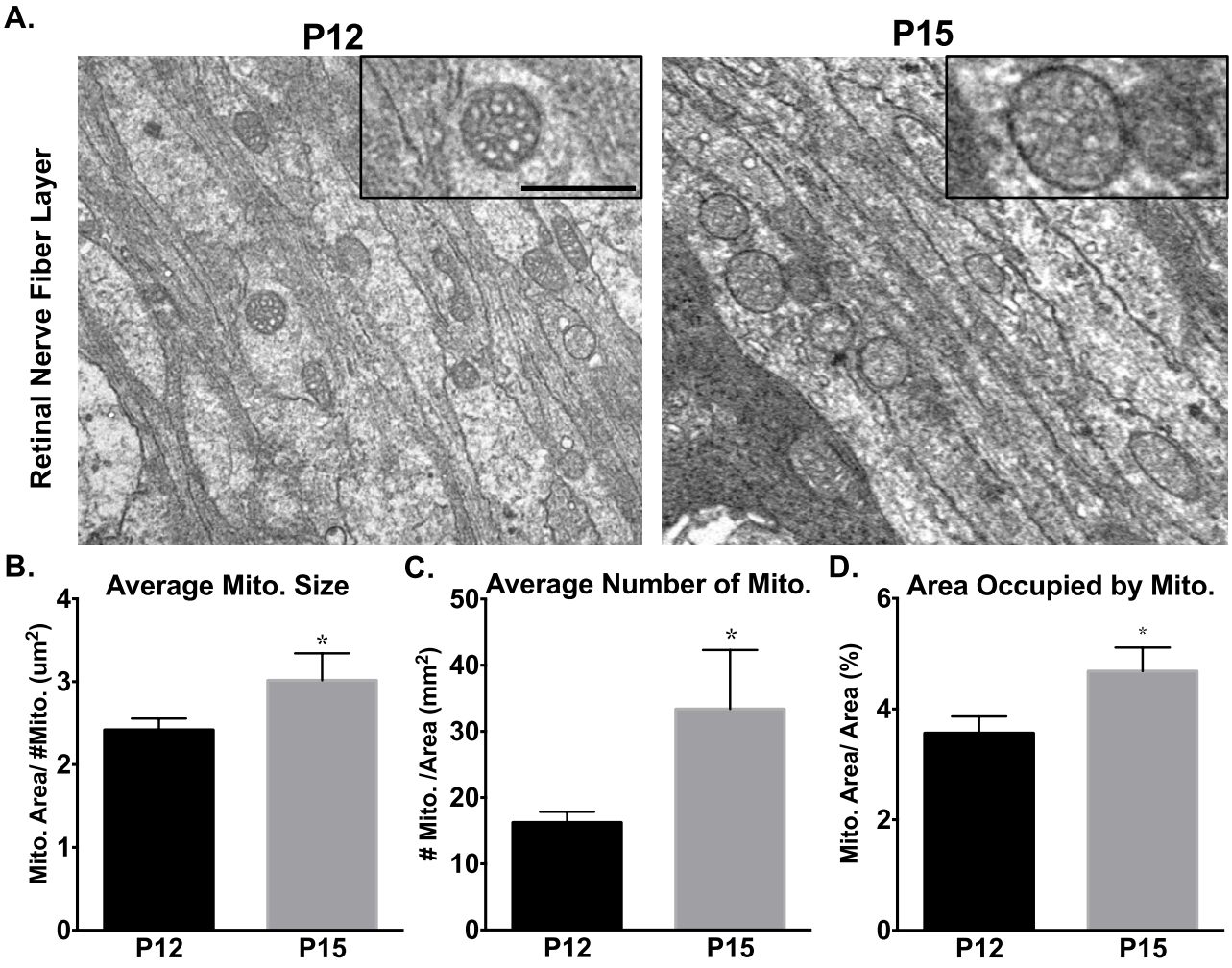

Figure 2. Mitochondrial size and number increase at eye opening in RGC axons. (A) Mitochondria were imaged and quantified in RGC optic nerve axons by transmission electron microscopy before (P12) and after (P15) eye opening. Increased magnification (insets) shows mitochondrial membrane, cristae, and representative mitochondrial size differences. Scale bar 500 nm. (B) Average mitochondrial size, (C) number and (D) area increased significantly between P12 and P15. (Error bars indicate SEM; n ≥ 30 sections; t-test * $p < 0.05$).

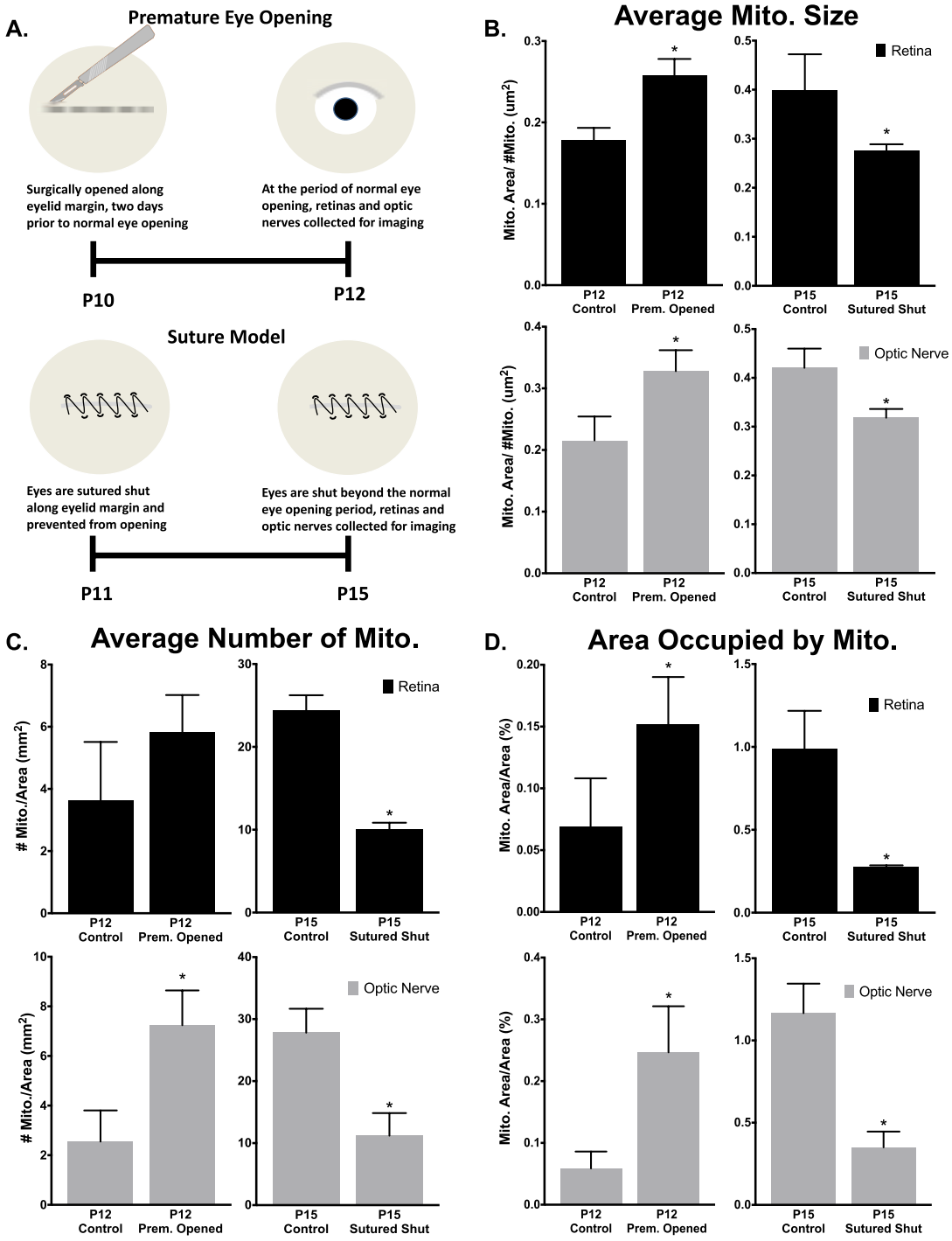

Figure 3. Eye opening is sufficient and necessary developmental changes in mitochondrial size and localization. **(**A) Surgical model for premature eye opening and sutured eyelid closure. (B) Average mitochondrial size, (C) number, and (D) area increase with premature eye opening, and this developmental increase is inhibited by prolonged eye closure. (Error bars indicate SEM; N≥ 3 mice per condition, 9 images analyzed per animal; Students t-test * $p < 0.05$.)

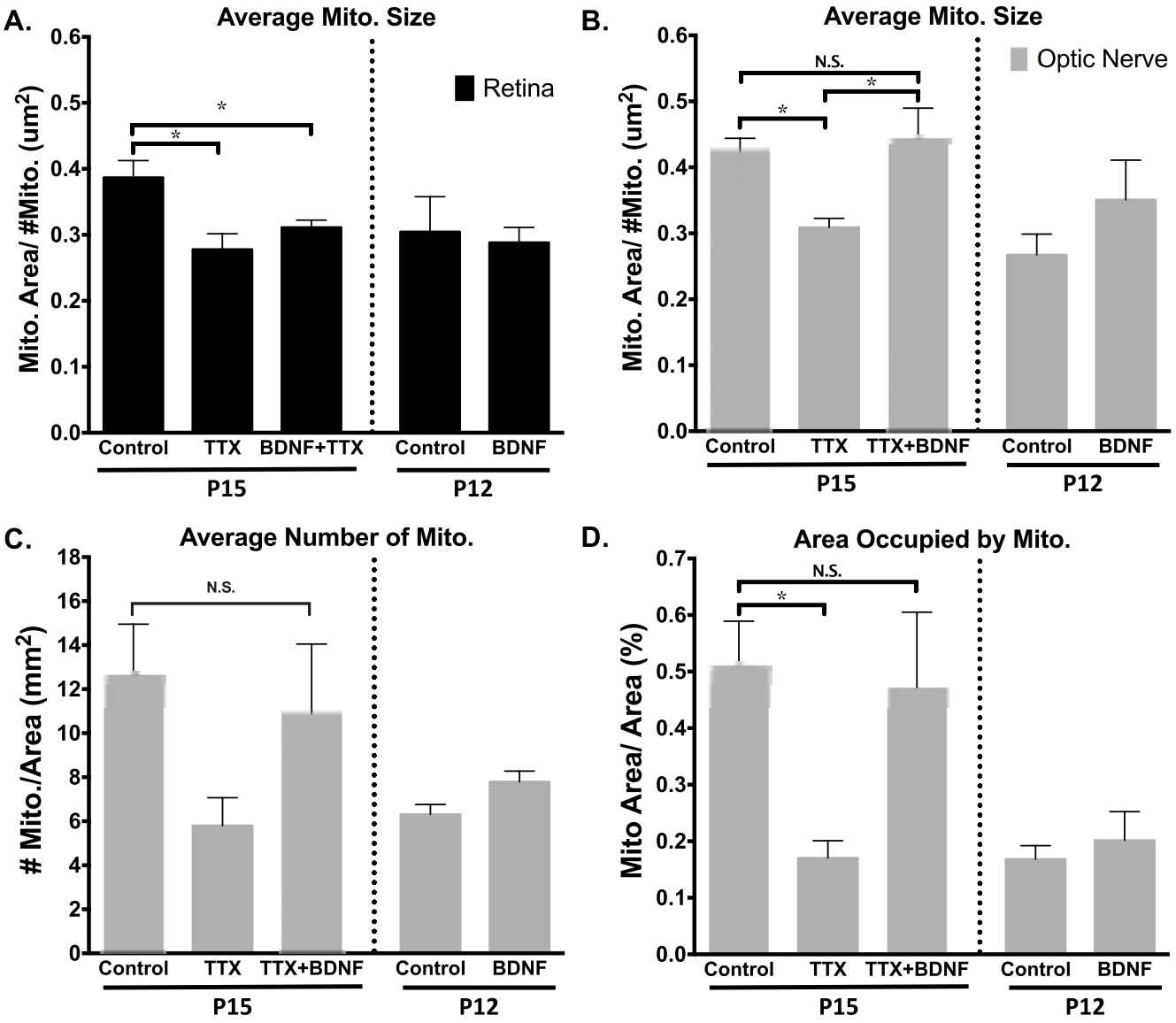

Figure 4. Mitochondrial developmental changes are dependent on retinal electrical activity and are partially rescued by BDNF in optic nerve axons. Control, TTX- or TTX plus BDNF-treated mice analyzed at P15, as well as control or BDNF-treated mice analyzed at P12 are graphed on the same axis for comparison, but the experiments were performed and analyzed separately. Measured changes in (A) average mitochondrial size within retinal axons and (B) optic nerve axons, as well as the corresponding mitochondrial (C) number and (D) area. (Error bars indicate SEM; N= 3 mice per condition, 9 images analyzed per animal; one-way ANOVA with Newman-Keuls multiple comparisons test (A-C) or Fisher LSD test (D), * $p < 0.05$)

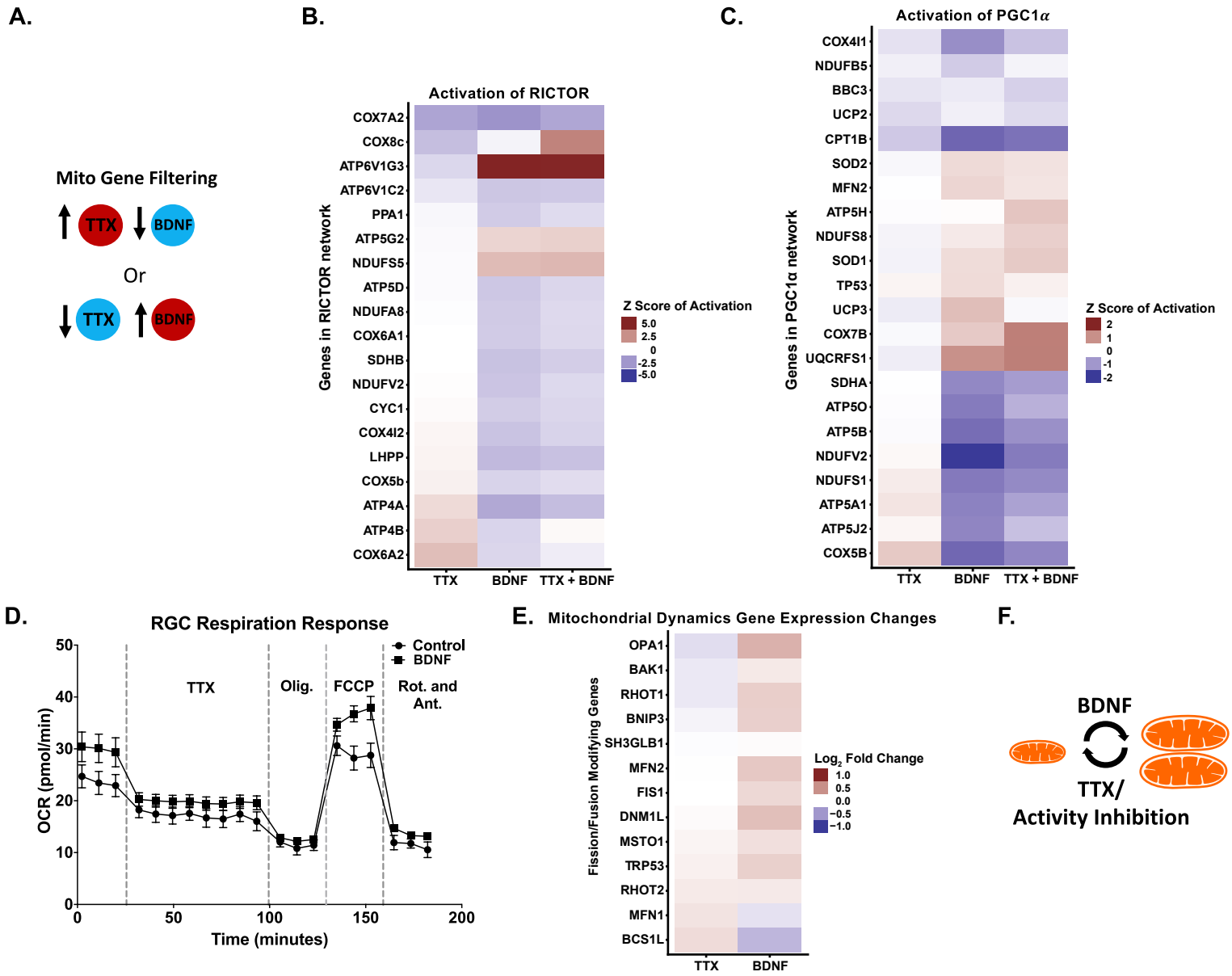

Figure 5. RGC nuclear-encoded mitochondrial gene expression in response to activity inhibition with TTX and/or BDNF is consistent with inhibition versus activation of mitochondrial dynamics and energetics. (A) Model for filtering data acquired from RT-PCR gene array analysis of P15 acutely purified RGCs, after TTX and/or BDNF intravitreal injections at P11 and P13 (N=3 RGC preps per condition). Filters were placed to identify gene expression regulated in opposing directions by BDNF and TTX. The resulting genes were then passed through IPA® pathway analysis software, which suggested 10 major upstream regulators, with PGC1- α and RICTOR at the top of the list. Downstream gene expression data modulated by these upstream regulators were transformed into Z-score of activation. Up- or downregulated gene sets are denoted by color.(B)Genes identified in our array that are regulated by RICTOR represent mainly energetics genes. (C) Genes identified in our array that are regulated by PGC1-α represent mainly mitochondrial dynamics and biogenesis regulators. (D) Measuring the effect of BDNF on mitochondrial dependent oxygen consumption in purified RGCs shows an increase in the basal respiration rate, and maximum respiration capacity (with FCCP addition) regardless of activity inhibition by TTX (introduced 35min after initial recording). TTX, Oligomycin, FCCP, and Rotenone/Antimycin A, were added sequentially at time points marked with vertical lines. Recorded values were acquired using the Seahorse XF96 instrument (Error bars indicate SEM; n=6 replicates per condition, pooled from 3 separate RGC preps and assayed on one plate) (E) Genes identified in our array that have been previously demonstrated as mitochondrial fission/fusion or mitochondrial size modifying are opposingly regulated by TTX and BNDF, with most genes upregulated by BDNF. (F) Model of the predicted mitochondrial events triggered by TTX or BDNF, based on gene pathway analysis and the identified mitochondrial changes in injected mice.

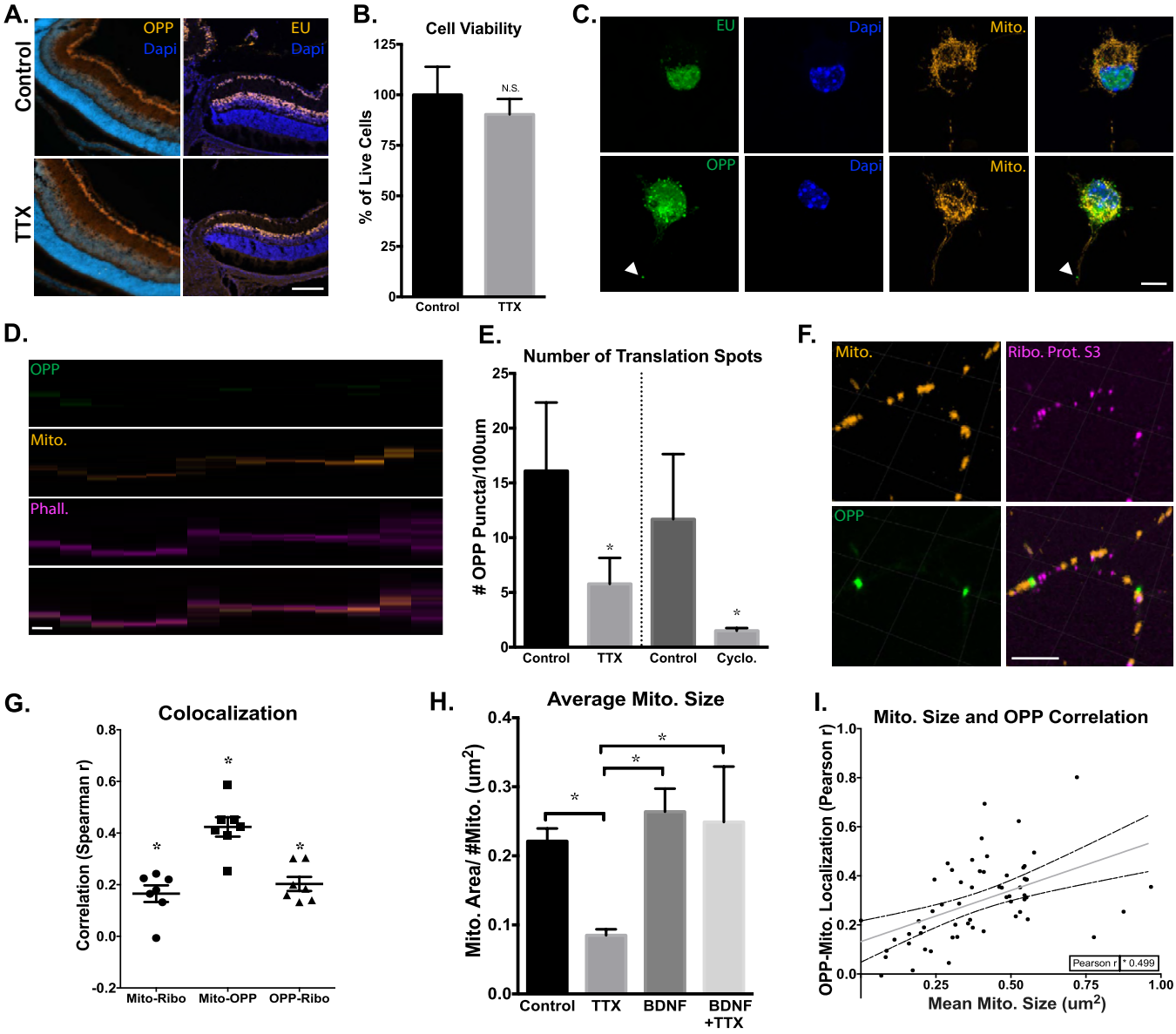

Figure 6. Activity regulates mitochondrial localized protein translation in axons. (A) Representative images collected by confocal microscope of P15 retinas, after in vivo intravitreal injections of TTX or BSS (control) at P11 and P13, and an injection of EU or OPP 2 hours before dissection and tissue processing. There were no detectable differences in EU or OPP fluorescence in the retina after TTX-mediated inhibition of activity (100um scale bar). (B) Cell viability of TTX- and-control treated RGCs, identified as Calcein-AM positive and Sytox negative, normalized for total cell number by Hoescht, and quantified as percent change relative to control treated cells (Error bars indicate SEM; N=3 replicate RGC preps, n>100 cells per replicate condition; Student's t-test, *p < 0.05.). (C) Confocal images of cultured RGCs treated with BacMam virus, labeling mitochondria with DsRed, and pulsed with EU for 1hr or OPP for 15 min before fixation and staining for newly synthesized RNA and protein, respectively. EU RNA and OPP protein staining were strongly detected in RGC nuclei and cell bodies, and newly translated proteins were also detected in axons (marked by arrows, 10um scale bar). (D) Axon tips demonstrate strong OPP+ puncta throughout growth cone and terminal axon domains. OPP-labeled with Alexa488, mitochondria with DsRed, and axon tips with phalloidin Alexa647 (5um scale bar). (E) Quantified average number of OPP puncta per 100 µm of P4 RGC's axon termini, treated with TTX or cycloheximide and with vehicle treated controls. Groups separated by vertical line were experimentally treated and analyzed separately (Error bars indicate SEM; n>10 randomly imaged axons, selected from 3 replicate RGC preps; Student's t-test, *p < 0.05). (F) Representative image of mitochondria, OPP-labeled new protein synthesis, and ribosomal protein S3 colocalization within axons (1um scale bar), along with (G) the spearman correlation values for the association of OPP to Mito, Mito to Ribosomes, and Ribosomes to OPP signals in line-scanned axons (Error bars indicate SEM; n=7 randomly imaged axons, selected from 3 replicate RGC preps; individual R values were all significant, * p < 0.05). (H) Quantified mean mitochondrial size in axons from RGCs incubated with TTX, BDNF, TTX and BDNF, or vehicle controls (Error bars indicate SEM; n>10 randomly imaged axons, from 3 replicate RGC preps; one-way ANOVA with Holm-Sidak's test, *p < 0.05). (I) Pearson's correlation values from a pixel by pixel analysis for OPP-mitochondrial colocalization relative to mean mitochondrial size, demonstrating a significant and positive correlation between increasing OPP colocalization and mitochondrial size (Regression line and 95% confidence intervals are plotted, data points from n>30 randomly imaged axons, selected from 3 replicate RGC preps; Pearson r was significant,*p < 0.05).

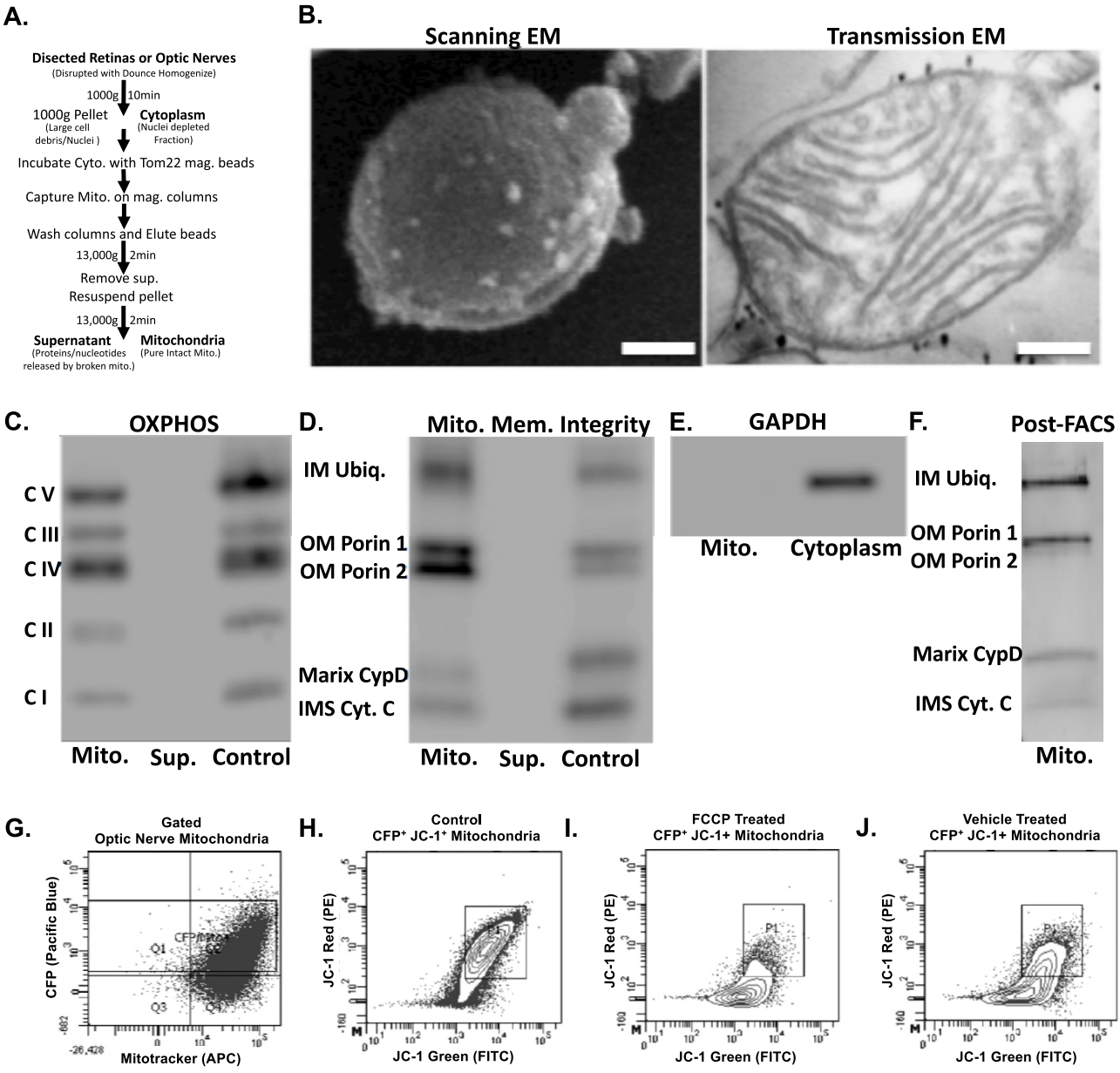

Figure 7. Purified mitochondria retain their protein content and membrane integrity. (A) Outline of mitochondrial isolation and subsequent assays. (B) TOM22-bound nanoparticles are visible, bound to the outer mitochondrial membrane in both SEM (white spots) and TEM (black dots). Scale bars 50 nm and 100 nm. (C-F) Western blot analyses of purified mitochondria and supernatants. Magnetically isolated mitochondria retain (C) OXPHOS subunits, as well as (D) outer membrane (OM), inner membrane (IM), and inner membrane space (IMS) proteins. (E) GAPDH is detectable in cytoplasmic but not mitochondrial isolate fractions. (F) FACS-sorted mitochondria retain both inner and outer membrane integrity proteins. (G) FACS-isolated mitochondria are intact and viable, retaining CFP and fluorescing with membrane potential-dependent mitotracker CMXROS. (H) Sorted CFP+ mitochondria demonstrate polarization-dependent fluorescence with JC-1, and (I) lose membrane potential with FCCP depolarization to a greater degree than (J) vehicle-treated controls.

A.

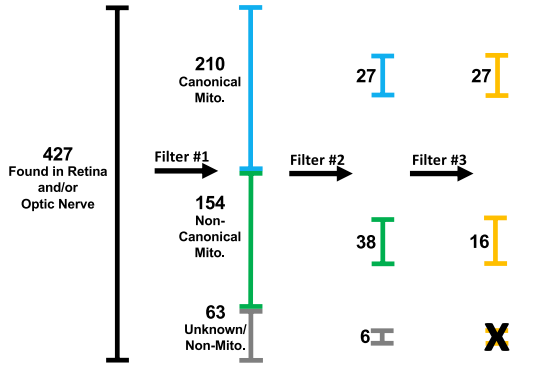

B. Isolated Mitochondria Proteome

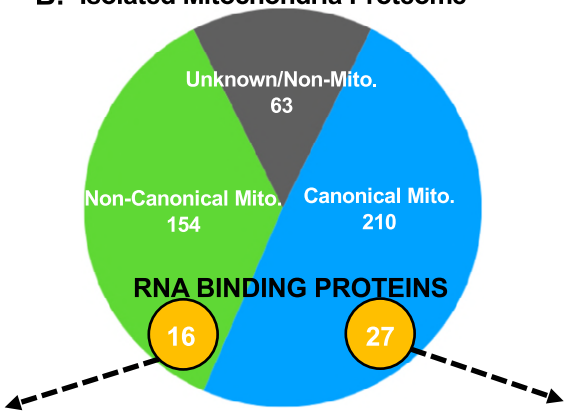

C.

Gene ID	Description	Mito. Evidence (PubMed IDs)	RNA Target	RNA Related Activity	Evidence for RNA Binding (PubMed IDs)
Anxa1	annexin A1	7750463; 10806526; 21886813	mRNA	RNA binding	22658674
Calr	calreticulin	28522876; 24813996; 25087122; 28522876; 2645096	mRNA	mRNA binding	22658674; 14726956
Canx	calnexin	18417615; 28522876; 20382740; 26450961	mRNA	mRNA binding	27452465; 22681889; 22658674
Ckap4	cytoskeleton-associated protein 4	22453275	mRNA	mRNA binding	22681889; 22658674; 27453046
Dnm1	dynamin 1	10559943;17884824	mRNA	mRNA binding	22681889
Dync1h1	dynein cytoplasmic 1 heavy chain 1	16467387; 15304525; 24492963	mRNA	mRNA binding	27452465; 22681889; 22658674; 27453046
Eef1a1	eukaryotic translation elongation factor 1 alpha 1	17853889; 21080726	tRNA/ mRNA	Translation	25365966; 22658674; 27453046; 22681889
Hnrnpk	heterogeneous nuclear ribonucleoprotein K	15485813; 11741984	mRNA	RNA binding, nuclease activity	21036867
Lrrc59	leucine rich repeat containing 59	21359316; 22447445	mRNA	RNA binding	22658674; 27453046
Pcbp1	poly(rC) binding protein 1	22105485	mRNA	mRNA processing	27452465; 22681889; 22658674; 27453046
Rpl18	ribosomal protein L18	25487825; 11959135; 22138184; 19858288; 25378625; 28827470	mRNA	Translational (Comp. of 60S Ribo.)	27452465; 27453046
Rpl22	ribosomal protein L22	25487825;11959135; 22138184; 19858288 25378625; 28827470	mRNA	Translational (Comp. of 60S Ribo.)	27452465; 22681889; 22658674; 27453046
Rplp2	ribosomal protein, large P2	25487825; 22138184; 11959135; 19858288; 25378625; 28827470	mRNA	Translational (Comp. of 60S Ribo.)	27452465; 27453046
Rps17	ribosomal protein S17	25487825; 11959135 22138184; 19858288 25378625; 28827470	mRNA	Translation (Comp. of 40S Ribo.)	27452465; 22681889; 22658674
Ywhag	tyrosine 3-monooxygenase/ tryptophan 5-monooxygenase activation protein, gamma polypeptide	16981892	mRNA	RNA binding	22658674; 27453046
Ywhaz	tyrosine 3-monooxygenase/ tryptophan 5-monooxygenase activation protein, zeta polypeptide	19289463; 22837806; 16981892	mRNA	RNA binding	22658674

D.

Gene ID	Description	Mito. Evidence (PubMed IDs)	RNA Target	RNA Related Activity	Evidence for RNA Binding (PubMed IDs)
Acaa2	acetyl-Coenzyme A acyltransferase 2 (mitochondrial 3-oxoacyl-Coenzyme A thiolase)	26450961	mRNA	RNA binding	22658674
Aldh6a1	aldehyde dehydrogenase family 6, subfamily A1	26450961	mRNA	RNA binding	22658674
Atp5a1	ATP synthase, H+ transporting, mitochondrial F1 complex, alpha subunit 1	26450961	mRNA	RNA binding	22658674; 27453046
Atp5b	ATP synthase, H+ transporting mitochondrial F1 complex, beta subunit	26450961	mRNA	RNA binding	22658674
Auh	AU RNA binding protein/enoyl-coenzyme A hydratase	26450961	mRNA	RNA processing	25365966; 7892223
C1qbp	complement component 1, q subcomponent binding protein	26450961	mRNA	RNA processing, Translation	19541640; 25365966
Exog	endo/exonuclease (5'-3'), endonuclease G-like	26450961	RNA	RNA binding, nuclease activity	25365966
Gatb	glutamyl-tRNA(Gln) amidotransferase, subunit B	26450961	tRNA	Translation	25365966
Got2	glutamate oxaloacetate transaminase 2, mitochondrial	26450961	mRNA	RNA binding	22681889; 27453046
Hadhb	hydroxyacyl-Coenzyme A dehydrogenase/3-ketoacyl-Coenzyme A thiolase/enoyl-Coenzyme A hydratase (trifunctional protein), beta subunit	26450961	mRNA	RNA binding	22658674; 27453046
Hsd17b10	hydroxysteroid (17-beta) dehydrogenase 10	26450961	tRNA/ mRNA	RNA binding	22681889
Hspe1	heat shock protein 1 (chaperonin 10)	26450961	mRNA	RNA binding	22658674; 27453046
Immt	inner membrane protein, mitochondrial	26450961	mRNA	RNA binding	22658674
Lars2	leucyl-tRNA synthetase, mitochondrial	26450961	tRNA	Mito. Translation	25365966
Lonp1	lon peptidase 1, mitochondrial	26450961	RNA	RNA binding	25365966; 14739292; 22658674
Lrpprc	leucine-rich PPR-motif containing	26450961	mRNA	RNA processing	25365966; 22658674; 27453046; 22681890; 12832482
Mdh2	malate dehydrogenase 2, NAD (mitochondrial)	26450961	mRNA	RNA binding	22681889; 22658674; 27453046
Mrpl19	mitochondrial ribosomal protein L19	26450961	mitochondrial ribosome	Mito. Translation	25365966; 27453046; 22658674
Mrpl49	mitochondrial ribosomal protein L49	26450961	mitochondrial ribosome	Mito. Translation	25365966
Mrps22	mitochondrial ribosomal protein S22	26450961	mitochondrial ribosome	Mito. Translation	25365966
Mrps27	mitochondrial ribosomal protein S27	26450961	mitochondrial ribosome	Mito. Translation	22658674; 25365966; 22841715
P4hb	prolyl 4-hydroxylase, beta polypeptide	26450961	mRNA	RNA binding	22681889; 22658674; 27453046
Slc25a11	solute carrier family 25 (mitochondrial carrier oxoglutarate carrier), member 11	26450961	mRNA	RNA binding	22681889
Slc25a5	solute carrier family 25 (mitochondrial carrier, adenine nucleotide translocator), member 5	26450961	mRNA	RNA binding	22658674
Tsfm	Ts translation elongation factor, mitochondrial	26450961	mRNA	Mito. Translation	22681889; 22658674; 25365966
Tst	thiosulfate sulfurtransferase, mitochondrial	26450961	rRNA	RNA transport	25365966
Tufm	Tu translation elongation factor, mitochondrial	26450961	mRNA	Mito. Translation	25365966; 27453046; 22658674

Figure 8. Proteomics mass spectrometry analysis reveals nuclear-encoded RNA binding proteins associated with purified mitochondria. (A) Filtering used to identify mitochondria-specific proteins and proteins with RNA binding properties.(B) Venn diagram of total protein hits sorted by annotation in the MitoCarta database. (C,D) Candidate mitochondria-associated RNA binding proteins with cited evidence (PubMed ID shown) for their functional RNA binding role and mitochondrial interaction (N=6 mitochondrial purifications).

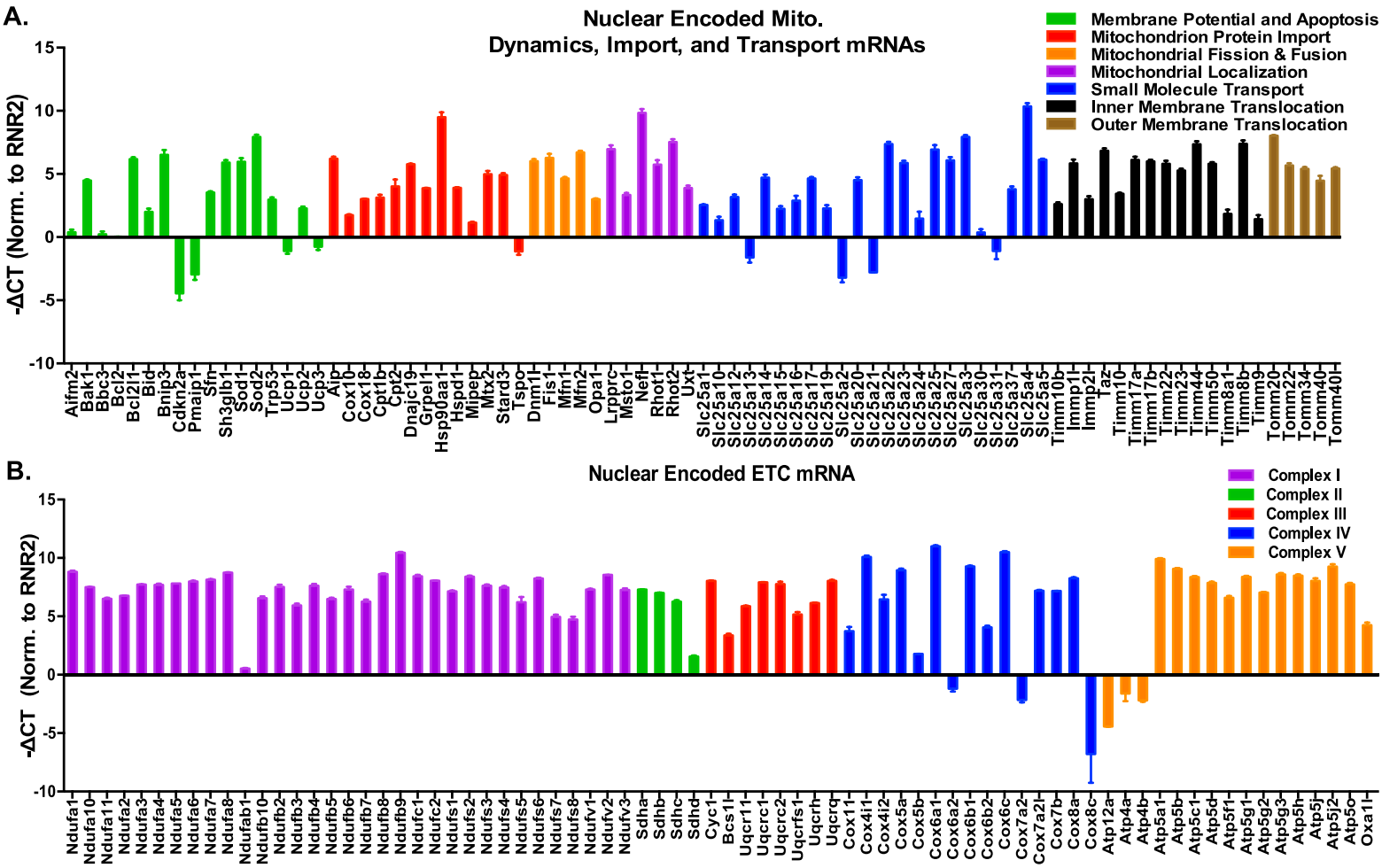

Figure 9. Isolated mitochondria bind nuclear-encoded RNAs associated with mitochondrial dynamics and energetics. (A) qRT-PCR array of mitochondrial dynamics and (B) energetics genes from purified mitochondria, normalized to RNR-2, a mitochondria-encoded ribosomal RNA(N=3 mito. purifications) . All CT values were pulled from amplifications well below 30 cycles. The data is presented as the inverse of the delta CT value, indicating more or less abundance of a particular nuclear encoded gene relative to RNR2. Genes are clustered by annotated functional roles in mitochondria.

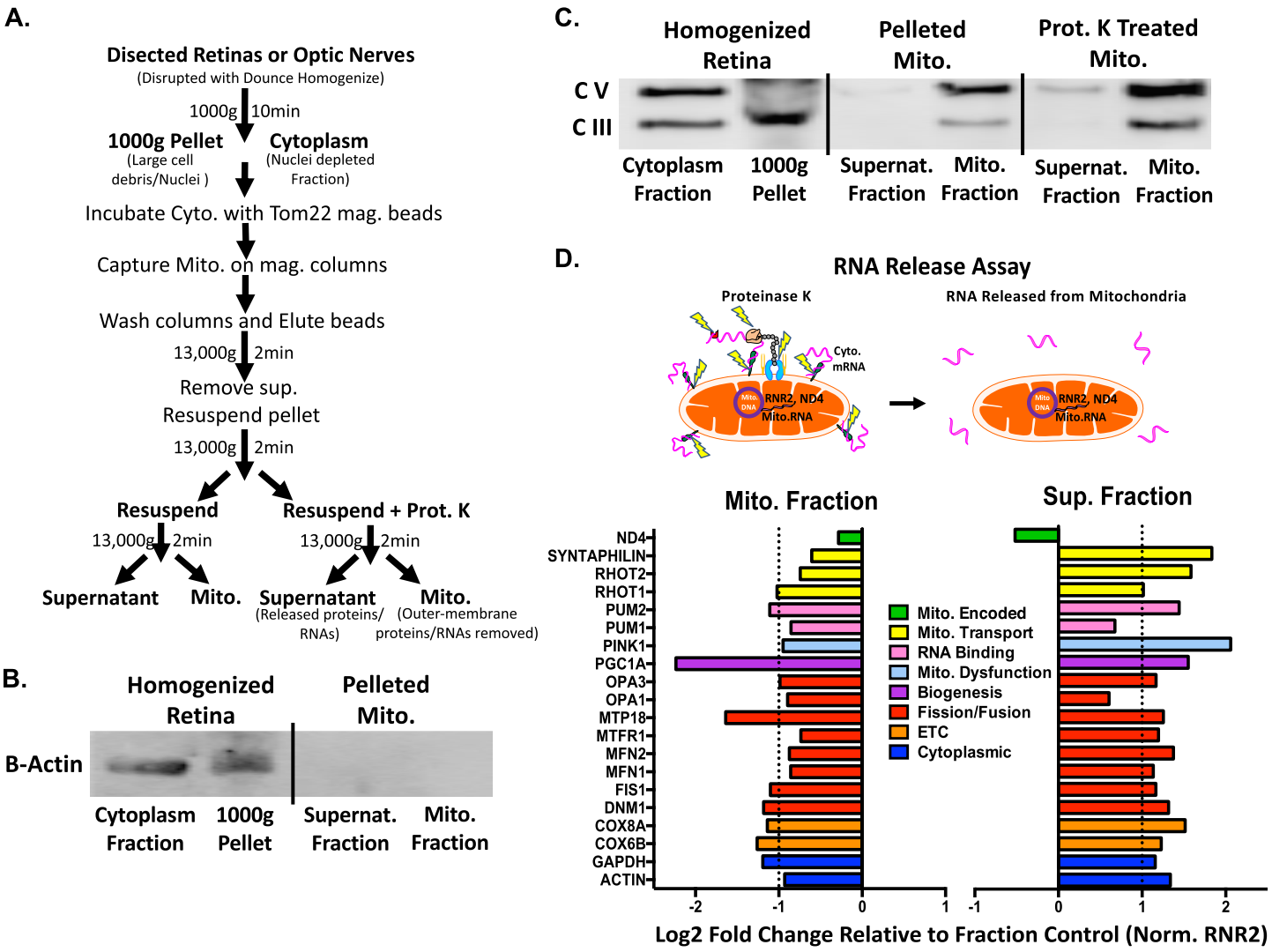

Figure 10. Purified mitochondria bind nuclear-encoded mRNAs through outer membrane-associated proteins. (A) Outline of mitochondrial isolation and subsequent assays. (B) β-actin is detected in homogenized retina but not in purified mitochondria. (C) Mitochondrial pellets treated with proteinase K retain inner matrix proteins, Complex III-Core Protein 2 (UQCRC2) and Complex V alpha subunit (ATP5A), confirming that proteinase K only strips off outer membrane-associated proteins. (D) Proteinase K-treated mitochondria release bound RNA into the supernatant fraction, as detected by qPCR of pelleted mitochondrial fraction and corresponding supernatant fractions. Data normalized to control mitochondrial fraction and RNR2, graphed as a log2 fold change to represent up and down regulation of RNA. Dotted line represents changes greater than 2-fold (n=3 replicates from a mito. purification).

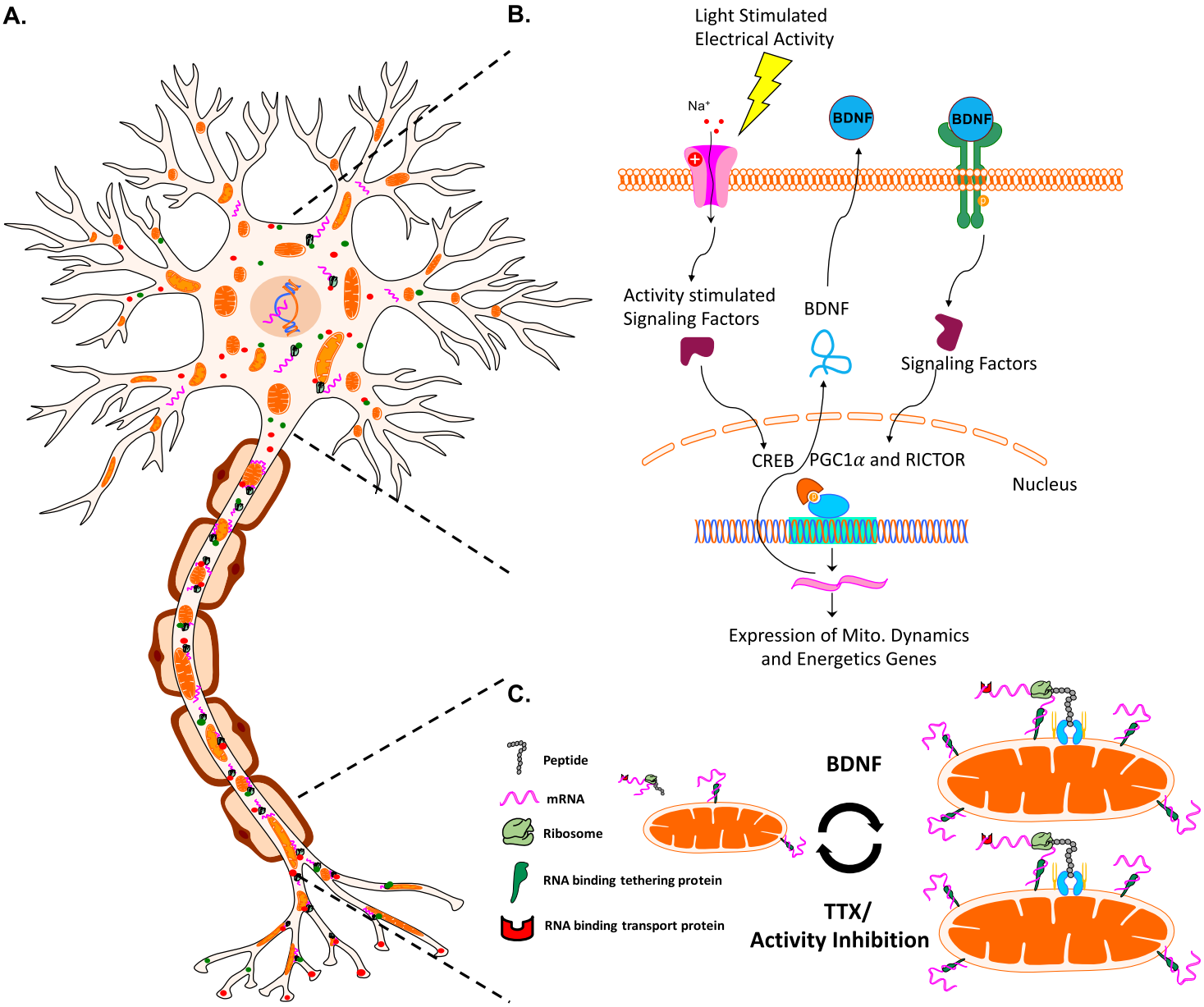

Figure 11. A model for activity- and BDNF-regulated mitochondrial size, number, and associated protein translation. (A) Neurons contain mitochondria, RNA, RNA binding and transport proteins, ribosomes, and newly synthesized proteins, throughout distal axon and dendrite compartments. (B) Electrical activity in RGCs, for example driven by light stimulation of retinal circuitry after eye opening, activates a signaling pathway that culminates in the activation of transcription factors such as CREB, and the expression of BDNF. BDNF signaling stimulates nuclear-encoded mitochondrial gene expression, coordinated by the activation of transcriptional regulators RICTOR and PGC1-α. (C) Neuronal activity and downstream BDNF signaling stimulates increases in mitochondrial size and number, reversed by activity inhibition. Changes in mitochondrial size also correlate with mitochondrial localized translation of nuclear-encoded transcripts.